



HAL
open science

The Release of Adipose Stromal Cells from Subcutaneous Adipose Tissue Regulates Ectopic Intramuscular Adipocyte Deposition

Amandine Girousse, Marta Gil-Ortega, Virginie Bourlier, Célia B Bergeaud, Quentin Sastourné-Arrey, Cédric Moro, Corinne Barreau, Christophe Guissard, Julie Vion, Emmanuelle Arnaud, et al.

► **To cite this version:**

Amandine Girousse, Marta Gil-Ortega, Virginie Bourlier, Célia B Bergeaud, Quentin Sastourné-Arrey, et al. The Release of Adipose Stromal Cells from Subcutaneous Adipose Tissue Regulates Ectopic Intramuscular Adipocyte Deposition. *Cell Reports*, 2019, 27 (2), pp.323-333.e5. 10.1016/j.celrep.2019.03.038 . hal-02136523

HAL Id: hal-02136523

<https://hal.science/hal-02136523>

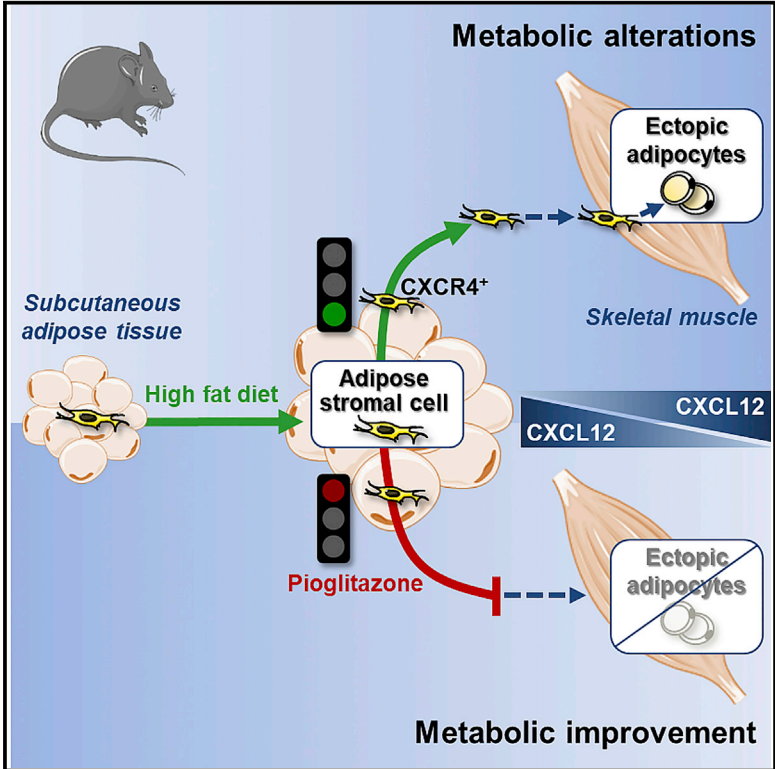
Submitted on 22 May 2019

HAL is a multi-disciplinary open access archive for the deposit and dissemination of scientific research documents, whether they are published or not. The documents may come from teaching and research institutions in France or abroad, or from public or private research centers.

L'archive ouverte pluridisciplinaire **HAL**, est destinée au dépôt et à la diffusion de documents scientifiques de niveau recherche, publiés ou non, émanant des établissements d'enseignement et de recherche français ou étrangers, des laboratoires publics ou privés.

The Release of Adipose Stromal Cells from Subcutaneous Adipose Tissue Regulates Ectopic Intramuscular Adipocyte Deposition

Graphical Abstract



Authors

Amandine Girousse, Marta Gil-Ortega, Virginie Bourlier, ..., Noémie Juin, Louis Castella, Coralie Sengenès

Correspondence

amandine.girousse@inserm.fr (A.G.), coralie.sengenès@inserm.fr (C.S.)

In Brief

Girousse et al. show that, in mice fed a high-fat diet, adipose stromal cells (ASCs) can egress subcutaneous adipose tissue and infiltrate skeletal muscle to form ectopic adipocytes, causing metabolic disturbance. ASC trafficking is regulated by the CXCR4/CXCL12 axis, and pioglitazone intermittent treatment can prevent muscle ectopic lipid deposition.

HIGHLIGHTS

- ASCs egress subcutaneous adipose tissue during dietary challenge
- ASCs infiltrate muscle and differentiate into adipocytes, disturbing metabolism
- Dietary-driven ASC trafficking relies on CXCL12 signals
- Pioglitazone can prevent dietary-driven ASC infiltration in muscle



The Release of Adipose Stromal Cells from Subcutaneous Adipose Tissue Regulates Ectopic Intramuscular Adipocyte Deposition

Amandine Girousse,^{1,*} Marta Gil-Ortega,¹ Virginie Boulrier,² Célia Bergeaud,¹ Quentin Sastourné-Arrey,¹ Cédric Moro,² Corinne Barreau,¹ Christophe Guissard,¹ Julie Vion,² Emmanuelle Arnaud,¹ Jean-Philippe Pradère,³ Noémie Juin,¹ Louis Casteilla,¹ and Coralie Sengenès^{1,4,*}

¹Stromalab, Université de Toulouse, CNRS ERL5311, EFS, INP-ENVT, INSERM U1031, Université Paul Sabatier, 31432 Toulouse, France

²Institut des maladies métaboliques et cardiovasculaires, Team 4, UMR1048, Université Paul Sabatier, 31432 Toulouse, France

³Institut des maladies métaboliques et cardiovasculaires, Team 3, UMR1048, Université Paul Sabatier, 31432 Toulouse, France

⁴Lead Contact

*Correspondence: amandine.girousse@inserm.fr (A.G.), coralie.sengenés@inserm.fr (C.S.)

<https://doi.org/10.1016/j.celrep.2019.03.038>

SUMMARY

Ectopic lipid deposition (ELD) is defined by excess fat storage in locations not classically associated with adipose tissue (AT) storage. ELD is positively correlated with insulin resistance and increased risk of metabolic disorders. ELD appears as lipid droplets or adipocytes, whose cell origin is unknown. We previously showed that subcutaneous AT (ScAT) releases adipocyte progenitors into the circulation. Here, we demonstrate that triggering or preventing the release of adipocyte precursors from ScAT directly promoted or limited ectopic adipocyte formation in skeletal muscle in mice. Importantly, obesity-associated metabolic disorders could be mimicked by causing adipocyte precursor release without a high-fat diet. Finally, during nutrient overload, adipocyte progenitors exited ScAT, where their retention signals (CXCR4/CXCL12 axis) were greatly decreased, and further infiltrated skeletal muscles. These data provide insights into the formation of ELD associated with calorie overload and highlight adipocyte progenitor trafficking as a potential target in the treatment of metabolic diseases.

INTRODUCTION

Adipose tissue (AT) has a remarkable capacity to expand to adapt to energy storage demand. With the expansion of both adipocyte size and number, namely adipocyte hypertrophy and hyperplasia, AT offers an appropriate response to calorie excess (reviewed in [Pellegriani et al., 2016](#)). Subcutaneous AT (ScAT) in male mice does not show significant adipocyte hyperplasia in response to obesogenic stimuli ([Jeffery et al., 2015](#); [Wang et al., 2013](#)). Moreover, with sustained positive energy balance, ScAT becomes dysfunctional due to a limited ability to form new adipocytes. Both observations lead to the ScAT “expandability theory,” whereby the expansion of ScAT has a defined

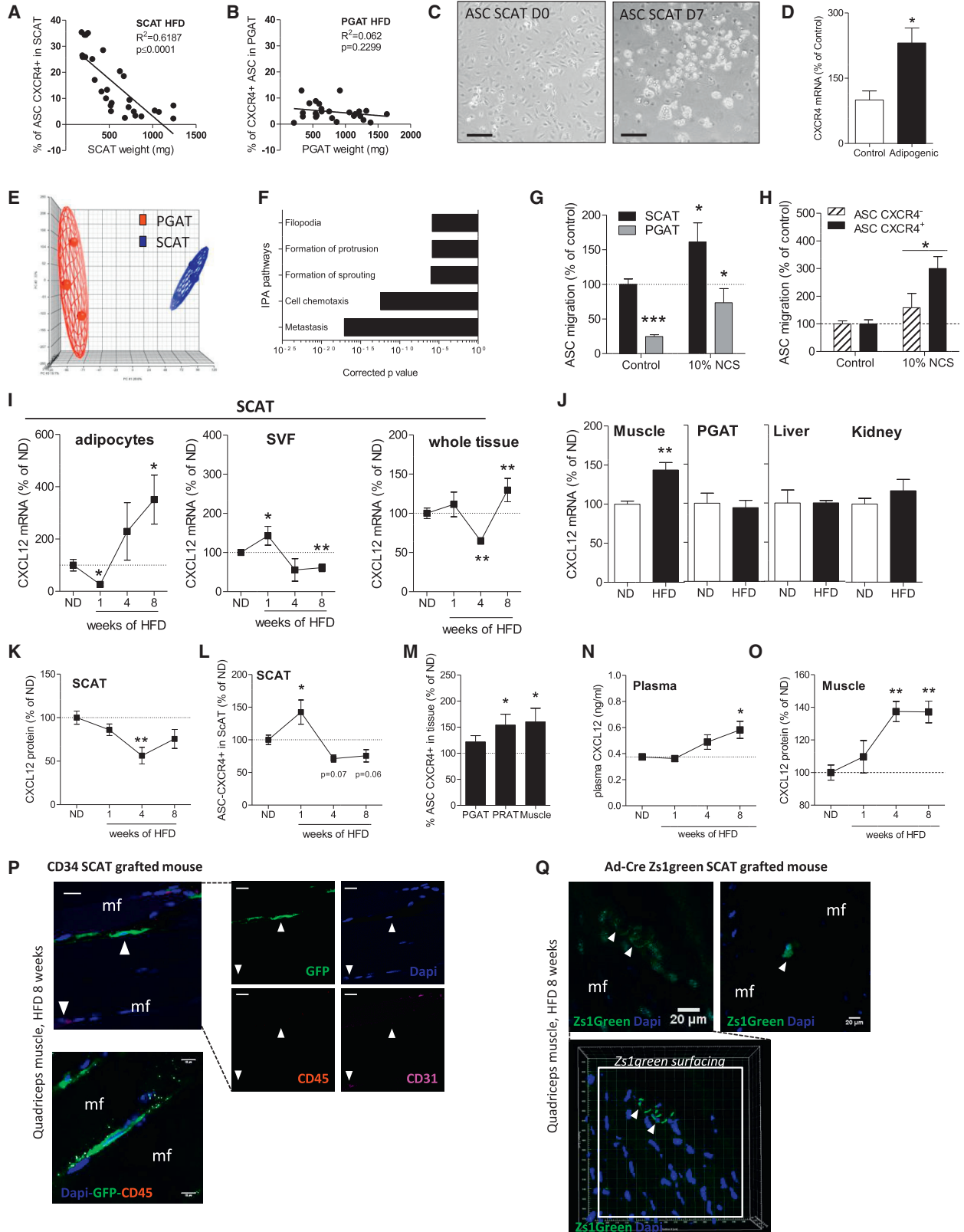
limit that is set individually ([Taylor and Holman, 2015](#); [Virtue and Vidal-Puig, 2008, 2010](#)). The parameters controlling such a set limit are varied (number of adipocyte progenitors, angiogenesis, and extracellular matrix remodeling capacities) and still not fully understood. Thus, lipids are no longer safely buffered into ScAT and accumulate into visceral depots as well as in non-AT sites, constituting ectopic lipid deposition (ELD).

ELD is widely documented in the form of lipid droplets within the functional parenchymal cells of several tissues such as skeletal muscles, liver, myocardium, or kidney ([de Vries et al., 2014](#); [Szendroedi and Roden, 2009](#)) resulting from two biological mechanisms: (1) take-up of circulating fatty acids and esterification into triglycerides and (2) *de novo* lipogenesis, both of which are well documented. It is now generally accepted that ELD is associated with lipotoxicity, insulin resistance, and metabolic disorders such as type 2 diabetes mellitus (T2DM) ([Laurens and Moro, 2016](#); [Lettner and Roden, 2008](#); [Shulman, 2000](#)) and perfectly exemplified in lipodystrophy, a rare extreme disorder characterized by massive ELD due to lack of AT ([Hussain and Garg, 2016](#)). In that sense, the development and fate of ELD represents a cornerstone in the pathophysiology of obesity-associated disorders. Of note, ELD can also take the form of proper adipocytes lodged between functional cells (in muscle [reviewed in [Hamrick et al., 2016](#)]), pancreas ([Pinnick et al., 2008](#); [Szendroedi and Roden, 2009](#)), renal sinus ([de Vries et al., 2014](#)), and epi- and pericardium ([Gaborit et al., 2013](#); [Shulman, 2014](#)), whose origin remains totally unknown.

Within AT, adipocytes originate from the differentiation of multipotent progenitors, termed adipose stromal cells (ASCs) ([Wang et al., 2013](#); [Zuk et al., 2002](#)). ASCs share specific features with their bone marrow (BM) counterparts, mesenchymal stromal cells (MSCs) ([Friedenstein et al., 1970](#); [Friedenstein et al., 1974](#)), such as cell surface marker combination, multilineage mesodermal differentiation potential, and paracrine and immunomodulation properties ([Mamus et al., 2011](#); [Rodeheffer et al., 2008](#); [Sengenès et al., 2007](#)). ASCs enable adipocyte turnover to allow their number to be relatively stable regardless of body fat mass evolution ([Spalding et al., 2008](#)).

The cellular origin and the mechanisms that control ectopic adipocyte formation have not been reported. Obesity has been





(legend on next page)

found to be associated with increased frequency of circulating MSCs (Bellows et al., 2011), and we recently found that ScAT releases ASCs into the circulation and that the chemokine CXCL12 and its receptor CXCR4 regulate this event (Gil-Ortega et al., 2013, 2014). This intriguing observation led us to hypothesize that ectopic adipocytes, which progressively develop during obesity, could arise from a release of ASCs from ScAT during exposure to a high-fat diet (HFD). To test our hypothesis, we deliberately provoked repeated ASC release by treating mice with a CXCR4 antagonist we previously used (AMD3100) (Gil-Ortega et al., 2013, 2014) and monitored the consequences on ectopic adipocyte formation. We show that HFD-enlarged ScAT induced the release of a specific subpopulation of ASCs from this depot and their infiltration into ectopic sites. Furthermore, in the absence of nutrient overload, causing the release of ASCs was by itself sufficient to mimic HFD-induced ectopic adipocyte formation in skeletal muscle together with the associated metabolic degradations.

RESULTS AND DISCUSSION

HFD Specifically Induces the Mobilization of CXCR4⁺ASCs from ScAT toward Skeletal Muscle

To investigate the impact of HFD on the ability of AT depots to release ASCs, mice were fed normal chow (normal diet [ND]) or an HFD for 8 weeks (Figures S1A–S1C). In ScAT, the proportion of CXCR4⁺ ASCs, ranging from 3% to 30% of total ASCs, was inversely correlated with fat pad weight enlarged with the HFD (Figure 1A). This change was specific to expanding ScAT because it was not found under the ND or in other AT depots such as perigonadal AT (PGAT) (Figure 1B), mesenteric AT, peri-renal AT, or BM (Figure S1D). The decrease in CXCR4⁺-ASC content with enlarged ScAT was not due to the loss of

CXCR4 expression when ASCs differentiate into adipocytes, because CXCR4 content was increased in ASCs cultured in pro-adipogenic media for 7 days (Figures 1C, 1D, and S1E). These findings suggest that ScAT enlargement is associated with the mobilization of CXCR4-expressing ASCs.

To understand such depot specificity, we used global microarray gene expression analysis of total ASCs (whatever their CXCR4 status) from ScAT and visceral AT (PGAT). Principal component analysis revealed clear gene expression profile segregation by tissue origin (Figure 1E). Ingenuity pathway analysis was used for functional annotation of the genes differentially expressed between the two depots. The highest-rated network showed the functions cell chemotaxis, metastasis, formation of sprouting and protrusion, and filopodia (Figure 1F). Cell chemotaxis was among the most enriched pathways ($p = 3.5 \times 10^{-13}$) and the heatmap clearly showed high expression of several genes involved in cell migration (Figure S1F) in ASCs from ScAT.

Finally, we compared the migratory function of ASCs from ScAT or PGAT and confirmed that ScAT ASCs showed increased basal and serum-activated migratory activity (50% and 30%, respectively) as compared with PGAT ASCs (Figure 1G). This migratory capacity was even larger in CXCR4-expressing ScAT ASCs (Figure 1H). Thus, these results illustrate ASC migration with depot-specific differences both at genetic and functional levels.

Progenitor or stem cell retention and release are largely governed by the binding of the chemokine CXCL12 to its receptor CXCR4, with high CXCL12 levels in the microenvironment favoring their retention versus low levels allowing their egress to circulation (Lapidot et al., 2005). Therefore, we investigated whether CXCL12 levels in total ScAT as well as its cellular components (adipocyte and stroma vascular fraction [SVF]) were modified as ScAT enlarged. The *cxcl12* mRNA expression in adipocytes

Figure 1. High-Fat Diet Specifically Induces the Mobilization of CXCR4⁺ ASCs from ScAT toward Skeletal Muscle

(A and B) Simple linear regression between percentage of CXCR4-expressing ASCs in stroma vascular fraction isolated from subcutaneous adipose tissue (ScAT) (A) and perigonadal AT (PGAT) (B) and tissue weight in mice fed a high-fat diet (HFD) for 8 weeks. R² and p values are presented on the graphs.

(C and D) Representative images (C) of ASCs isolated from ScAT and cultivated in normal medium or after 7 days in pro-adipogenic media and CXCR4 mRNA expression (D). Scale bar, 50 μ m.

(E) Representative principal component analysis of gene expression in ASCs isolated from ScAT (blue) and PGAT (red) for three different mice and subjected to Affymetrix analysis.

(F) Ingenuity pathway analysis of top-scored pathways.

(G and H) *In vitro* ASC migration assay of ASCs isolated from ScAT or PGAT (G) and from ScAT only and sorted for their CXCR4 status (H). Graphs present the number of ASCs that migrated into the lower chamber as a percentage of the control condition. NCS, newborn calf serum.

(I) Time course of mRNA expression of *cxcl12* in isolated adipocytes, stroma vascular fraction, and whole ScAT in mice fed an HFD.

(J) Time course of mRNA expression of *cxcl12* in other organs (quadriceps muscle, PGAT, liver, and kidney) in mice fed an HFD for 4 weeks.

(K) Time course of CXCL12 protein expression in ScAT. Values were obtained in ng/g of tissue and normalized to the normal diet (ND) group. ND value is 0.51 ± 0.08 ng/g.

(L) Time course of CXCR4-expressing ASCs in ScAT. Population was numbered as a percentage of CXCR4-expressing ASC in total ASCs, normalized to ND group.

(M) Percentage of CXCR4-expressing ASCs in ectopic sites, normalized to ND group after 8 weeks of protocol.

(N) Time course of CXCL12 plasma level.

(O) Time course of CXCL12 protein level in quadriceps muscle. Values were obtained in ng/g of tissue and normalized to ND group. ND value is 1.15 ± 0.22 ng/g.

(P) Confocal immunofluorescence image of a representative quadriceps muscle section of two HFD-fed animals. Agarose-embedded sections were immunostained with antibodies for CD45 and CD31. Nuclei were stained with DAPI. mf, muscle fibers. Arrowheads point to ASCs. Scale bar, upper panel is for 20 μ m, lower panel is for 10 μ m.

(Q) Confocal immunofluorescence image of a representative quadriceps muscle section of HFD-fed animals. Agarose-embedded sections were only stained with DAPI. Lower panel shows surfacing of Zs1green adipocytes with Imaris. Scale bar, 20 μ m.

(A, B, E, F, G, and N) $n = 5-18$; data are mean \pm SEM. (C and D) $n = 5-7$ of three independent experiments; data are mean \pm SEM. One-way ANOVA Dunn's post-tests; * $p \leq 0.05$, ** $p \leq 0.01$, and *** $p \leq 0.001$ compared to ND or control condition. (G and H) Two-way ANOVA Bonferroni post-test.

See also Figures S1 and S2.

first decreased early during the HFD before increasing significantly at later stages, whereas the *cxcl12* mRNA expression in the SVF showed the reverse pattern and in less proportions (Figure 1I). In total ScAT, the *cxcl12* mRNA expression mimicked that of adipocytes with a slight delay (Figure 1I) but was significantly increased in quadriceps muscle (Figure 1J). These variations were specific because they were not observed in other tissues such as PGAT, liver, and kidney (Figure 1J). The protein level of CXCL12 was significantly reduced in ScAT during the HFD (Figure 1K), which favored CXCR4⁺-ASC detachment from ScAT during its enlargement. We then examined the content of total ASCs, the ASC-CXCR4⁺ subpopulation, and their proliferative activity over time in ScAT. The ASC-CXCR4⁺ number increased rapidly under the HFD (Figure 1L) with no change in proliferation (Figure S1I) before greatly decreasing at later stages of the diet. Variations in ASC-CXCR4⁺ number appeared specific because changes in total ASC content in ScAT followed a strict opposite pattern (Figures S1G and S1H) and were not observed in PGAT (Figures 1M, S1G, and S1I). However, the ASC-CXCR4⁺ number was concomitantly increased in ectopic sites such as perirenal adipose tissue (PRAT) and muscle (Figure 1M), but their proliferation was not modified (Figures S1G–S1I). Also, we found increases in CXCL12 content in plasma (Figure 1N) and CXCL12 protein level in muscle (Figure 1O) over time.

We next aimed to visualize ASC trafficking and ectopic relocation under the HFD. However, no mouse model is available to visualize trafficking of native ASCs from AT to other tissues because of the lack of a unique specific ASC marker. To overcome this technical limitation, we used Tg(Cd34-EGFP) MF6Gsat/Mmcd mice (called CD34-GFP, an ASC surface marker) from which a piece of ScAT was grafted into the ScAT of a non-GFP recipient mouse (Figures S2A and S2B). Mice were then fed an HFD for 8 weeks. GFP-CD34⁺/Sca1⁺/CD45⁻/CD31⁻ cells were found on the immunohistochemistry of the quadriceps muscle (corresponding to ASCs; see Figures 1P, S2C, and S2D), which demonstrates that in response to an HFD, ASCs detach from ScAT and relocate ectopically in muscle. Because CD34 expression is lost when ASC enters adipogenic differentiation, we could not show that infiltrated CD34-GFP⁺ ASCs could differentiate to proper adipocytes. To further demonstrate that relocated ASCs could functionally differentiate into ectopic adipocytes, we grafted ScAT from B6.Cg-Gt(ROSA)26Sortm6(CAG-ZsGreen1)Hze/J × C57BL/6-Tg(Adipoq-cre/ERT2)1Soff/J mice (called Ad-Cre/Zs1Green) into wild-type (WT) mice (Figures S2E and S2F). Grafted mice were treated with tamoxifen after 8 weeks of an HFD to uncover the presence of ectopic adipocytes specifically differentiated from infiltrated ASCs (originating from the SCAT graft) (Figure S2F). Zs1Green-positive adipocytes were found in quadriceps muscles of HFD-fed mice but were missing in ND-fed mice (Figure 1Q), so ScAT-originating ASCs infiltrating the muscle of mice on an HFD can differentiate into adipocytes and participate in ectopic deposition. In another situation of adiposity (intramuscular glycerol injection [Pisani et al., 2010]), not caused by dietary intervention (unpublished data of our laboratory), we quantified that the infiltrated ASCs participate in up to 10% of the total fibro-adipogenic progenitors (FAPs) in the muscle. Further investigations are needed to measure the proportion of infiltrated ASCs differ-

entiating into adipocytes, revealing the quantitative importance of each progenitor pool in the development of adipocyte formation into the skeletal muscle and associated metabolic complications.

Recurrent ASC Release from ScAT Mimics Diet-Induced Obesity and Associated Disorders by Promoting Both Ectopic AT Depot Enlargement and Muscle Ectopic Adipocyte Formation

We postulated that provoking the repeated release of ASCs from ScAT should promote ectopic adipocyte formation and mimic the HFD-mediated features. Since we previously showed that the CXCR4 antagonist AMD3100 triggered the release of ASCs by ScAT as soon as 30 min and up to 3 h after drug administration (Gil-Ortega et al., 2013, 2014), we scheduled a protocol with one weekly AMD3100 injection for eight consecutive weeks. Control groups received injections of NaCl 0.9% vehicle and were fed an ND or HFD. As expected, 24 h after AMD3100 injection, the ScAT CXCR4⁺-ASC population was decreased 70% (Figure 2A). After 8 weeks of AMD3100 treatment, ND-fed mice showed higher body weight gain and total fat mass than mice fed an ND alone (Figures S3A and 2B); a similar pattern was also observed under an HFD. Lean mass was not affected by the treatment or the diet or their combination (Figure S3B). Surprisingly, ScAT and PGAT enlargement was not markedly affected (Figures 2C and 2D). Fat mass increase was not attributable to AMD3100-dependent adipogenesis because neither ASC (positive or not for CXCR4) proliferation (Figure S3C and S3D) nor their *in vitro* adipogenic differentiation was affected by AMD3100 treatment (Figure 2E). Food intake was slightly (4%) but significantly increased (Figure 2F), but neither energy expenditure nor activity was modified (Figures 2G and 2H) (respiratory quotient was slightly decreased over the night period [Figure 2I]). Because CXCR4 adipocyte-specific knockout animals show increased brown AT (BAT) mass associated with weight gain on dietary challenge (Yao et al., 2014), we investigated BAT in AMD3100-treated animals. BAT was also enlarged (data not shown).

These small changes in energy balance could explain per se the body weight gain in ND-fed mice treated with AMD3100, but the preferential relocation of this energy surplus in ectopic storage sites was surprising. CXCR4 is a key regulator of hematopoiesis, and AMD3100 is used in clinics to mobilize hematopoietic stem cells to peripheral blood (DiPersio et al., 2009). Thus, we verified the absence of medullar aplasia (Figure S3E) and immune-cell content modifications in blood and AT, the latter potentially altering obesogenic adipogenesis. We also found no modifications of immune-cell content in ScAT (Figure S3F), BM (Figure S3G), or blood (Figure S3H). In contrast to ScAT and PGAT, ectopic adipose depots such as mesenteric, peri-cardiac, and peri-aortic AT (Figure 2J) were all significantly increased with AMD3100 treatment almost to the extent of the HFD condition, and the combination of both an HFD+ADM3100 further exacerbated the phenotype. ND-fed AMD3100-treated mice also showed heavier quadriceps (Figure 2K) comparable to the HFD condition, but kidney, lung, and liver weights (Figure 2K) were not affected by the treatment or the diet, which shows the tissue specificity of the AMD3100 effect. Several

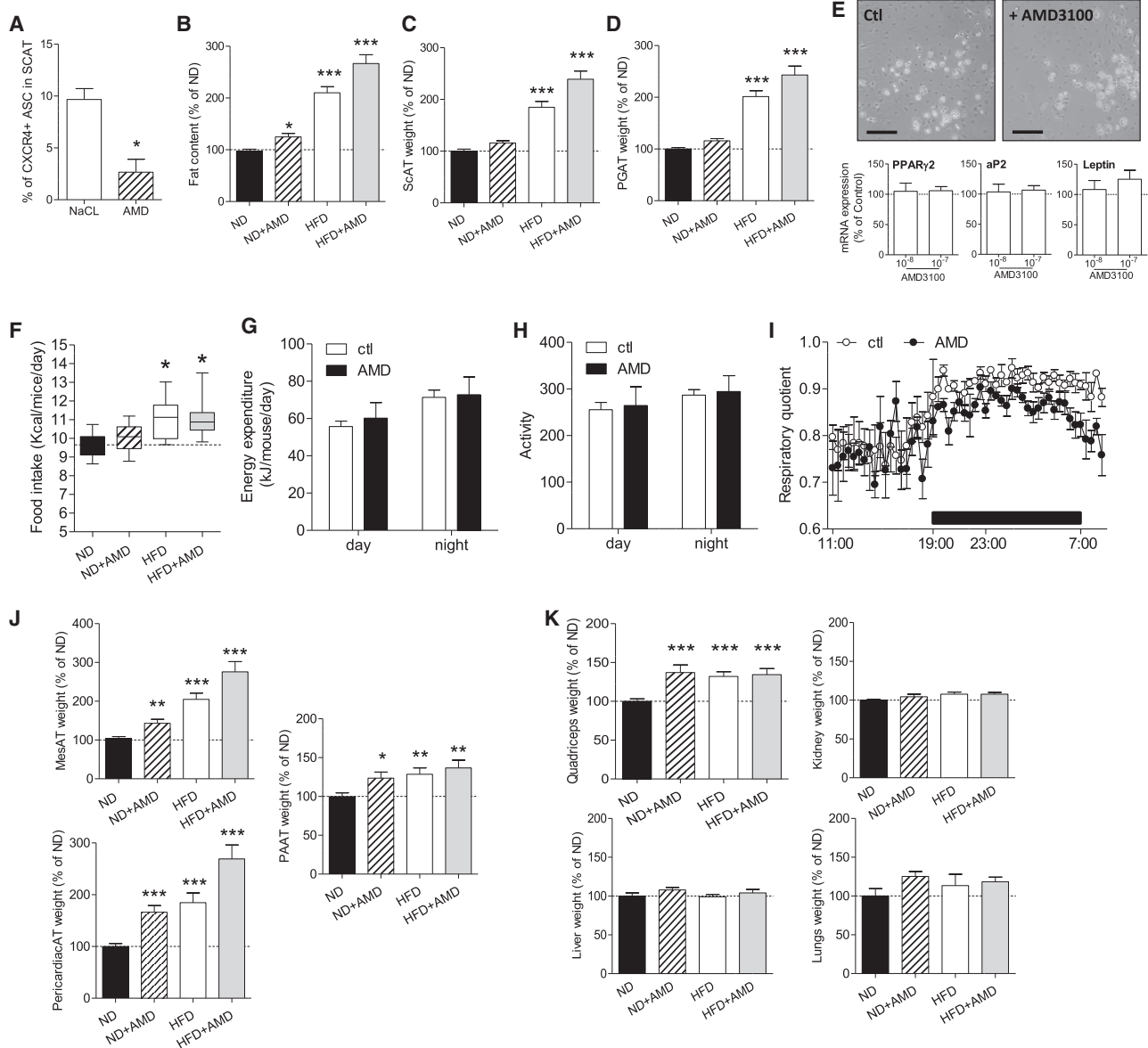


Figure 2. AMD3100 Treatment Promotes Ectopic Fat Deposition

Mice were fed an ND or HFD for 8 weeks and injected weekly with vehicle NaCl 0.9% or AMD3100.

(A) Percentage of CXCR4-expressing ASCs in ScAT 24 h after intra-peritoneal AMD3100 injection.

(B) Fat content after 8 weeks of protocol.

(C and D) Weight of ScAT (C) and PGAT (D).

(E) Representative images of ScAT stroma vascular fraction cultivated in normal medium or pro-adipogenic media supplemented or not with AMD3100 for 3 days. mRNA expression of PPAR γ 2, aP2, and leptin assessed at day 3 of differentiation. Scale bar, 50 μ m.

(F) Food intake measurement. Horizontal line is median, box edges are interquartile range, and whiskers are range.

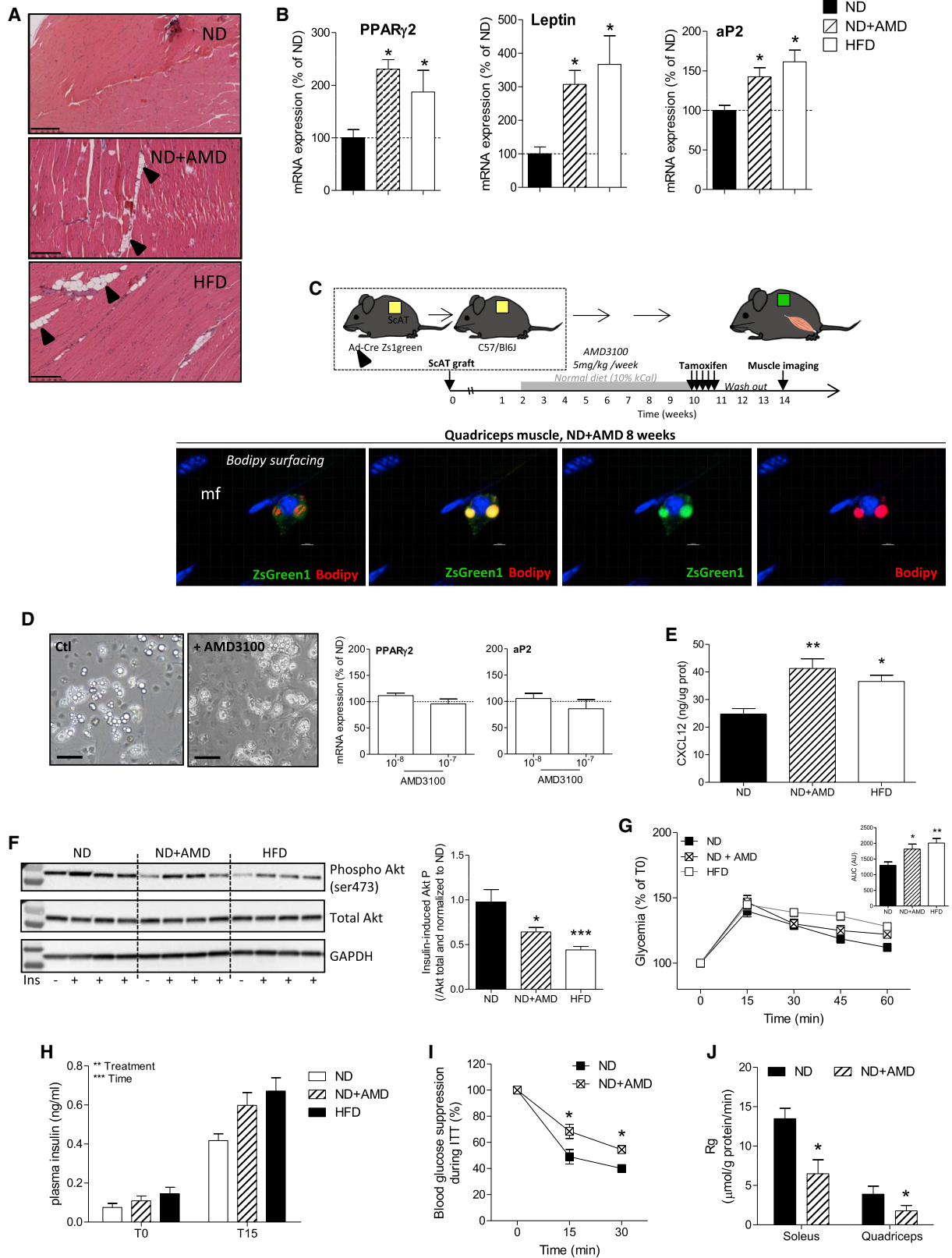
(G–I) Indirect calorimetry performed over a 24-h period. Energy expenditure (G), activity (H), and respiratory quotient (I) were measured individually in animals fed an ND and treated with AMD3100 or NaCl for 4 weeks.

(J) Adipose tissue weight: mesenteric, peri-cardiac, and peri-aortic AT (PAAT).

(K) Non-adipose tissue weight: quadriceps muscle, kidney, liver, and lungs after 8 weeks of protocol.

(A–D, F, J, and K) $n = 13$ –16. (E) $n = 5$ –7 of three independent experiments; data are mean \pm SEM unless indicated. One-way ANOVA Dunn's post-tests; * $p \leq 0.05$, ** $p \leq 0.01$, and *** $p \leq 0.001$ compared to ND or control condition.

See also Figure S2.



(legend on next page)

clusters of adipocytes were observed in the quadriceps of AMD3100-treated mice (Figure 3A), but no adipocytes were observed in ND-fed animals. In parallel, we detected increased expression of adipocyte markers (Figure 3B), to an extent comparable to the HFD condition. In an inducible mouse model specifically expressing Zs1Green protein in adipocytes (adiponectin promoter driven), clusters of fluorescent adipocytes appeared in AMD3100-treated animals after tamoxifen treatment (Figure S3I and S3J). To indeed verify the origin of such ectopic adipocytes, WT mice were grafted with Ad-Zs1Green-ScAT, fed an ND, and treated weekly with AMD3100 for 8 weeks before observing tamoxifen-induced adipocytes (Figure 3C). Zs1Green-positive small adipocytes appeared within the quadriceps muscle of AMD3100-treated mice (Figure 3C), which confirms that infiltrated ASCs could form proper ectopic adipocytes. The relative importance of ectopic adipocyte formation from ScAT ASCs versus local progenitors (fibro-adipogenic progenitors described in the pioneering works of Joe et al. [2010] and Uezumi et al. [2010]) remains to be assessed. Of note, as for ASCs in ScAT, AMD3100 did not per se trigger adipogenesis of local resident fibro-adipogenic progenitors (Figure 3D). Importantly and comparable to the HFD, AMD3100 treatment significantly increased the mRNA (Figure S3K) and protein expression of CXCL12 in muscle (Figure 3E), which rendered skeletal muscle attractive for circulating ASCs.

Muscle lipid storage in the form of adipocytes is well known to cause insulin resistance; however, the metabolic consequences of proper adipocyte infiltration are not well understood (Laurens and Moro, 2016; Shulman, 2014). Therefore, to investigate the metabolic consequences of such ectopic adipocyte accumulation in the muscle, freshly extracted soleus muscle was stimulated by insulin, which decreased levels of Ser473-phosphorylated Akt in AMD3100-treated mice (Figure 3F) and supports a deterioration of insulin signaling similar to that observed with the HFD. Increased GTT-related area under the curve (Figure 3G) as well as plasma insulin before and 15 min after glucose injection (Figure 3H) also revealed whole-body glucose intolerance with AMD3100 treatment comparable to the HFD condition, which was independent of direct effects of AMD3100 on glycaemia (Figure S3L). Finally, an insulin tolerance test with [3 H]deoxyglucose revealed both reduced blood glucose sup-

pression (Figure 3I) and reduced glucose uptake by quadriceps and soleus muscle (Figure 3J) in ND+AMD3100-treated mice versus ND alone.

Thus, AMD3100 treatment, causing recurrent release of ASCs into the circulation led to a remarkable physiological condition that was sufficient per se to alter fat mass and global metabolism without any diet intervention. The increased circulation of ASCs can by itself promote ectopic adipocyte formation, without any dietary signals, with circulating ASCs attracted to ectopic sites. Whether ASC infiltration is a consequence or cause of increased CXCL12 production remains to be determined. Of note, migrating ASCs do enter adipogenesis in ectopic sites as if local metabolic conditions or specific signals invited them. Levi et al. (2013) demonstrated greater adipogenic differentiation abilities for lymphedema-associated than ScAT-derived ASCs. Because we already demonstrated that ASCs leave ScAT via the lymphatics (Gil-Ortega et al., 2014; Figure S3M), circulating ASCs could be primed toward adipocyte differentiation during lymphatic trafficking and would be more prone to enter adipogenesis when infiltrating ectopic sites (Levi et al., 2013). These data show that repeated pharmacological triggering of ASC release induces ectopic adipocyte formation and metabolic perturbations without any dietary signals.

Pioglitazone Treatment Limits HFD-Induced ASC Liberation from ScAT and the Associated Ectopic Adipocyte Formation

Apart from well-established adipogenic and metabolic actions, peroxisome proliferator-activated receptor gamma (PPAR γ) agonists have evolved as cancer metastasis suppressors because they reduce tumor cell invasion, migration, and metastasis via a CXCR4-dependant pathway (Fenner and Elstner, 2005; Han and Roman, 2007; Kotta-Loizou et al., 2012; Kramer et al., 2016; Qin et al., 2014; Richard and Blay, 2007). Thus, we hypothesized that thiazolidinediones (TZDs) could limit ASC mobilization, as demonstrated in various cancer models. As for cancer cells, native ASCs isolated from ScAT and cultured with the antidiabetic drug pioglitazone for 24 h showed a significant decrease in spontaneous and serum-oriented migration (Figure 4A), which suggested an ability of pioglitazone to modulate ASC release and migration *in vivo*. While unconventional,

Figure 3. AMD3100 Treatment Increases Muscle Adipocyte Deposition Impairing Glucose Tolerance

Mice were fed an ND or HFD for 8 weeks then injected weekly with vehicle NaCl 0.9% or AMD3100.

(A) Histology of quadriceps muscle after 8 weeks of protocol; black arrowheads point to clusters of adipocytes. Scale bar, 250 μ m.

(B) mRNA expression of adipocyte markers (PPAR γ 2, aP2, and leptin) in quadriceps muscle.

(C) Experimental protocol scheme and confocal immunofluorescence images of a representative quadriceps muscle section of HFD-fed animals with tamoxifen treatment. Agarose-embedded sections were stained with Bodipy and DAPI. Scale bar, 10 μ m.

(D) Representative images of fibro-adipogenic progenitors (FAPs) isolated from total quadriceps muscle and cultivated in normal medium or pro-adipogenic media supplemented or not with AMD3100 for 3 days. mRNA expression of PPAR γ 2 and aP2 assessed at day 3 of differentiation. Scale bar, 20 μ m.

(E) CXCL12 protein level in quadriceps muscle.

(F) Western blot analysis and quantification of phospho- and total Akt in soleus muscle after *ex vivo* insulin stimulation; results were normalized to ND group.

(G and H) Glucose tolerance test and corresponding area under the curve (AUC) (G) and plasma insulin level (H) before (T0) and 15 min (T15) after glucose injection.

(I) Blood glucose suppression during insulin tolerance test (ITT).

(J) Tissue-specific glucose clearance by soleus and quadriceps muscles during ITT.

(A, B, D, and G) n = 10–14. (D) n = 5–7 of three independent experiments. (I–J) n = 3–5; data are mean \pm SEM. One-way ANOVA Dunn's post-test; *p \leq 0.05, **p \leq 0.01, and ***p \leq 0.001 compared to ND or control condition.

See also Figures S2 and S3.

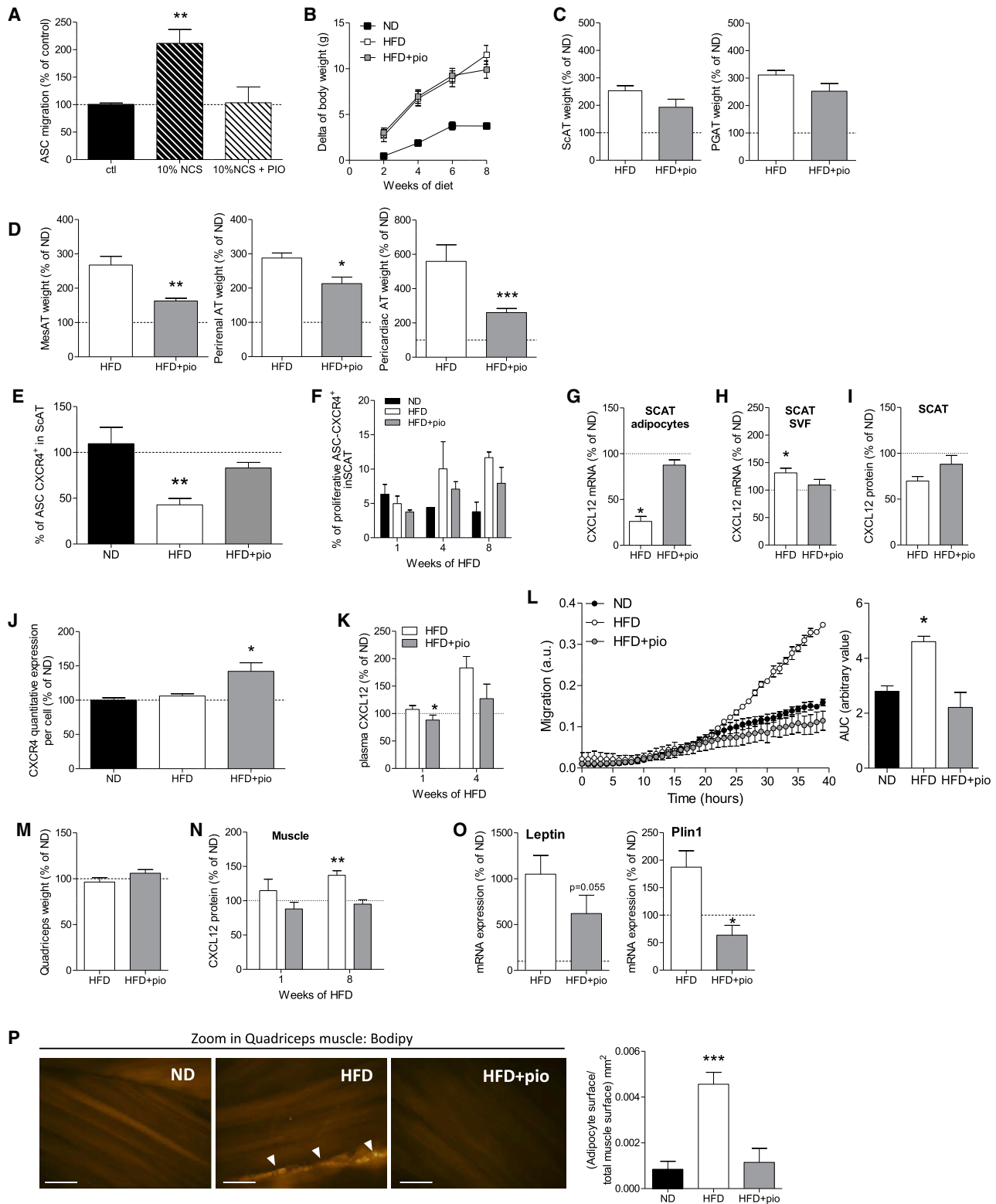


Figure 4. Pioglitazone Reduces Migratory Ability of ASCs *In Vitro* and HFD-Mediated Ectopic Lipid Deposition *In Vivo*

Mice were fed an ND or HFD for 1 or 8 weeks then injected weekly with DMSO vehicle or pioglitazone.

(A) *In vitro* migration assay of ASCs isolated from ScAT and cultivated for 24 h with pioglitazone 100 μ M or control DMSO and expressed as percentage of control DMSO.

(legend continued on next page)

we deliberately administered pioglitazone, once weekly (and not daily) for up to eight consecutive weeks to mice; first to avoid TZD-mediated adipogenesis (Soccio et al., 2014) (Figures S4A–S4C) and second to mimic the ADM3100 experimental procedure. Control groups received DMSO vehicle injections and were fed an ND or HFD. Under an HFD, neither food intake (Figure S4D) nor total body weight (Figure 4B) was affected by pioglitazone treatment. After 8 weeks of treatment, pioglitazone did not significantly modify HFD-induced enlargement of ScAT and PGAT (Figure 4C) but greatly limited ectopic adipose depot growth (mesenteric, perirenal, and peri-cardiac AT) (Figure 4D), with no effect on the weights of other tissue (Figure S4E). Of interest, the HFD-mediated decrease in the CXCR4⁺-ASC population between 1 and 8 weeks did not occur with pioglitazone treatment (Figure 4E). This finding was not supported by changes in ASC proliferation (Figure 4F), which suggests less mobilization. Moreover, after 1 week of an HFD, the HFD-mediated decrease in CXCL12 mRNA in adipocytes (Figure 4G) and increase in SVF (Figure 4H) did not occur with pioglitazone treatment. The total ScAT CXCL12 protein expression was less affected by the HFD (Figure 4I) and the CXCR4 quantitative expression per cell was significantly increased in ASCs from ScAT with pioglitazone treatment (Figure 4J), altogether suggesting higher ASC retention capacity. Moreover, the plasma level of CXCL12 was reduced with pioglitazone treatment (Figure 4K), and the *in vitro* migration ability of ASCs toward plasma was decreased with pioglitazone treatment as compared with the HFD (Figure 4L). Pioglitazone thus increased ASC anchoring factors in ScAT while decreasing plasmatic attractive signals, which led us to speculate that muscle could be less infiltrated by ectopic adipocytes. Indeed, we did not observe the expected increase in quadriceps muscle mass under the HFD (Figure 4M), and CXCL12 protein expression in muscle was decreased with pioglitazone treatment (Figure 4N). Furthermore, gene expression of specific adipocyte markers (leptin and *perilipin 1*; Figure 4O) in total quadriceps muscle was significantly reduced with pioglitazone treatment. Finally, the ectopic adipocyte proportion was decreased in animals treated weekly with pioglitazone (Figures 4P, S4F, and S4G). Overall, these experiments clearly demon-

strate that pioglitazone treatment limited ectopic adipocyte formation in muscle, the drug possibly acting at two levels: first by increasing ASC retention in ScAT and second by reducing ASC migratory ability toward attracting signals.

In summary, we show that modulating the release of ASCs from ScAT directly affects ectopic adipocyte deposition in muscle in mice. Ongoing studies focus on demonstrating that such adipocyte ectopic formation is not restricted to skeletal muscle. It is now well established that ScAT overgrowth is mainly hypertrophic rather than hyperplastic, although it contains large amounts of adipocyte progenitors (Jeffery et al., 2015; Wang et al., 2013). Intriguingly, ScAT-derived adipocyte progenitors readily form adipocytes *in vitro*, but ScAT adipogenesis *in vivo* seems limited. Our findings showing that ScAT releases adipocyte progenitors toward ectopic sites suggest that ScAT could bypass this expandability limitation and allow non-AT organs to store lipids in a competent cell. Whether this process is less metabolically threatening as compared with lipid droplet formation remains an open and major question of therapeutic importance.

STAR★METHODS

Detailed methods are provided in the online version of this paper and include the following:

- KEY RESOURCES TABLE
- CONTACT FOR REAGENT AND RESOURCE SHARING
- EXPERIMENTAL MODEL AND SUBJECT DETAILS
- METHOD DETAILS
 - Animal treatments
 - Isolation of the Stroma Vascular Fraction (SVF) from AT and BM and quadriceps muscle
 - Adipose Stem Cell (ASC) Sorting, Adipogenic Differentiation and Transwell Migration Assay
 - Flow Cytometry
 - Proliferation assay
 - Adipose Tissue Immunohistochemistry
 - RNA Isolation and Real-Time RT-PCR Analysis
 - Microarray Transcriptome Hybridization and Analysis

(B) Body weight gain.

(C) Weight of ScAT and PGAT.

(D) Weight of ectopic adipose depots (mesenteric, peri-renal, and peri-cardiac AT).

(E) CXCR4-expressing ASCs in ScAT after 8 weeks of protocol. The dotted line represents ND level at 1 week of protocol.

(F) Time course of ASC proliferation in ScAT.

(G–I) The *cxcl12* mRNA expression in isolated ScAT adipocytes (G), stroma vascular fraction (H), and whole tissue (I) after 1 week of protocol.

(J) Quantitative flow cytometry of CXCR4 expression per cell in ASCs from ScAT after 1 week of protocol.

(K) Plasma CXCL12 level after 1 week of protocol.

(L) *In vitro* ASC migration assay (Incucyte technology) toward plasma (8 weeks of protocol) with ND, HFD, or HFD+pioglitazone. Results are presented as arbitrary units and area under the curve (AUC).

(M) Quadriceps muscle weight after 8 weeks of protocol.

(N) CXCL12 protein content in quadriceps muscle after 1 and 8 weeks of protocol.

(O) mRNA expression of adipocyte-specific genes (leptin and *perilipin1*) in quadriceps muscle after 8 weeks of protocol.

(P) Representative immunofluorescence image of total quadriceps muscle section and quantification of Bodipy fluorescence. White arrowheads point to clusters of adipocytes. Scale bar, 500 μ m.

(A) $n = 5$ –8 of three independent experiments. (B–K and M–O) $n = 5$ –8. (L) $n = 3$. Data are mean \pm SEM. Student's *t* test and one-way ANOVA Dunn's post-test; * $p \leq 0.05$, ** $p \leq 0.01$, and *** $p \leq 0.001$ compared to ND or control condition.

See also Figure S4.

- Protein Extraction and Western Blot and ELISA Analysis
- QUANTIFICATION AND STATISTICAL ANALYSIS
- DATA AND SOFTWARE AVAILABILITY

SUPPLEMENTAL INFORMATION

Supplemental Information can be found online at <https://doi.org/10.1016/j.celrep.2019.03.038>.

ACKNOWLEDGMENTS

The authors thank US006/CREFRE INSERM/UPS (Toulouse, France), the platform of experimental histopathology, and the zootechnical core facility (Anexplo-Génotoul platform) for their technical assistance. We also thank the TRI-Genotoul imaging platform (Toulouse, France). We especially thank Mireille André and Yannick Jeanson for their excellent technical support. We are grateful to Professor Antonio Vidal-Puig for the insightful scientific discussions. This work was supported by the Fondation pour la Recherche Médicale (C.S. 2013) and Ligue Nationale contre le Cancer (C.S. 2010).

AUTHOR CONTRIBUTIONS

A.G., M.G.-O., V.B., L.C., and C.S. designed the study. A.G., M.G.-O., V.B., C.B., Q.S.-A., C.M., C.B., C.G., E.A., J.V., J.-P.P., N.J., and C.S. conducted experiments. A.G., M.G.-O., V.B., L.C., and C.S. analyzed and interpreted data. A.G., L.C., and C.S. wrote and edited the manuscript. All authors reviewed the final draft of the manuscript.

DECLARATION OF INTERESTS

The authors declare no competing interests.

Received: April 9, 2018

Revised: December 30, 2018

Accepted: March 11, 2019

Published: April 9, 2019

REFERENCES

- Badin, P.M., Vila, I.K., Louche, K., Mairal, A., Marques, M.A., Bourlier, V., Tavernier, G., Langin, D., and Moro, C. (2013). High-fat diet-mediated lipotoxicity and insulin resistance is related to impaired lipase expression in mouse skeletal muscle. *Endocrinology* *154*, 1444–1453.
- Bellows, C.F., Zhang, Y., Simmons, P.J., Khalsa, A.S., and Kolonin, M.G. (2011). Influence of BMI on level of circulating progenitor cells. *Obesity (Silver Spring)* *19*, 1722–1726.
- de Vries, A.P., Ruggenti, P., Ruan, X.Z., Praga, M., Cruzado, J.M., Bajema, I.M., D'Agati, V.D., Lamb, H.J., Pongrac Barlovic, D., Hojs, R., et al.; ERA-EDTA Working Group Diabetesity (2014). Fatty kidney: emerging role of ectopic lipid in obesity-related renal disease. *Lancet Diabetes Endocrinol.* *2*, 417–426.
- DiPersio, J.F., Uy, G.L., Yasothan, U., and Kirkpatrick, P. (2009). Plerixafor. *Nat. Rev. Drug Discov.* *8*, 105–106.
- Fenner, M.H., and Elstner, E. (2005). Peroxisome proliferator-activated receptor-gamma ligands for the treatment of breast cancer. *Expert Opin. Investig. Drugs* *14*, 557–568.
- Friedenstein, A.J., Chailakhjan, R.K., and Lalykina, K.S. (1970). The development of fibroblast colonies in monolayer cultures of guinea-pig bone marrow and spleen cells. *Cell Tissue Kinet.* *3*, 393–403.
- Friedenstein, A.J., Deriglasova, U.F., Kulagina, N.N., Panasuk, A.F., Rudakowa, S.F., Luriá, E.A., and Rudakow, I.A. (1974). Precursors for fibroblasts in different populations of hematopoietic cells as detected by the in vitro colony assay method. *Exp. Hematol.* *2*, 83–92.
- Gaborit, B., Abdesselam, I., and Dutour, A. (2013). Epicardial fat: more than just an “epi” phenomenon? *Horm. Metab. Res.* *45*, 991–1001.
- Gil-Ortega, M., Garidou, L., Barreau, C., Maumus, M., Breasson, L., Tavernier, G., García-Prieto, C.F., Bouloumié, A., Casteilla, L., and Sengenès, C. (2013). Native adipose stromal cells egress from adipose tissue in vivo: evidence during lymph node activation. *Stem Cells* *31*, 1309–1320.
- Gil-Ortega, M., Fernandez-Alfonso, M.S., Somoza, B., Casteilla, L., and Sengenès, C. (2014). Ex vivo microperfusion system of the adipose organ: a new approach to studying the mobilization of adipose cell populations. *Int. J. Obes.* *38*, 1255–1262.
- Hamrick, M.W., McGee-Lawrence, M.E., and Frechette, D.M. (2016). Fatty infiltration of skeletal muscle: Mechanisms and comparisons with bone marrow adiposity. *Front. Endocrinol. (Lausanne)* *7*, 69.
- Han, S., and Roman, J. (2007). Peroxisome proliferator-activated receptor gamma: a novel target for cancer therapeutics? *Anticancer Drugs* *18*, 237–244.
- Hussain, I., and Garg, A. (2016). Lipodystrophy syndromes. *Endocrinol. Metab. Clin. North Am.* *45*, 783–797.
- Jeffery, E., Church, C.D., Holtrup, B., Colman, L., and Rodeheffer, M.S. (2015). Rapid depot-specific activation of adipocyte precursor cells at the onset of obesity. *Nat. Cell Biol.* *17*, 376–385.
- Joe, A.W., Yi, L., Natarajan, A., Le Grand, F., So, L., Wang, J., Rudnicki, M.A., and Rossi, F.M. (2010). Muscle injury activates resident fibro/adipogenic progenitors that facilitate myogenesis. *Nat. Cell Biol.* *12*, 153–163.
- Kotta-Loizou, I., Giaginis, C., and Theocharis, S. (2012). The role of peroxisome proliferator-activated receptor- γ in breast cancer. *Anticancer. Agents Med. Chem.* *12*, 1025–1044.
- Kramer, K., Wu, J., and Crowe, D.L. (2016). Tumor suppressor control of the cancer stem cell niche. *Oncogene* *35*, 4165–4178.
- Lapidot, T., Dar, A., and Kollet, O. (2005). How do stem cells find their way home? *Blood* *106*, 1901–1910.
- Laurens, C., and Moro, C. (2016). Intramyocellular fat storage in metabolic diseases. *Horm. Mol. Biol. Clin. Investig.* *26*, 43–52.
- Lettner, A., and Roden, M. (2008). Ectopic fat and insulin resistance. *Curr. Diab. Rep.* *8*, 185–191.
- Levi, B., Glotzbach, J.P., Sorkin, M., Hyun, J., Januszzyk, M., Wan, D.C., Li, S., Nelson, E.R., Longaker, M.T., and Gurtner, G.C. (2013). Molecular analysis and differentiation capacity of adipose-derived stem cells from lymphedema tissue. *Plast. Reconstr. Surg.* *132*, 580–589.
- Maumus, M., Peyrafitte, J.A., D'Angelo, R., Fournier-Wirth, C., Bouloumié, A., Casteilla, L., Sengenès, C., and Bourin, P. (2011). Native human adipose stromal cells: localization, morphology and phenotype. *Int. J. Obes.* *35*, 1141–1153.
- Pellegrinelli, V., Carobbio, S., and Vidal-Puig, A. (2016). Adipose tissue plasticity: how fat depots respond differently to pathophysiological cues. *Diabetologia* *59*, 1075–1088.
- Pinnick, K.E., Collins, S.C., Londos, C., Gauguier, D., Clark, A., and Fielding, B.A. (2008). Pancreatic ectopic fat is characterized by adipocyte infiltration and altered lipid composition. *Obesity (Silver Spring)* *16*, 522–530.
- Pisani, D.F., Bottema, C.D., Butori, C., Dani, C., and Dechesne, C.A. (2010). Mouse model of skeletal muscle adiposity: a glycerol treatment approach. *Biochem. Biophys. Res. Commun.* *396*, 767–773.
- Qin, L., Gong, C., Chen, A.M., Guo, F.J., Xu, F., Ren, Y., and Liao, H. (2014). Peroxisome proliferator-activated receptor γ agonist rosiglitazone inhibits migration and invasion of prostate cancer cells through inhibition of the CXCR4/CXCL12 axis. *Mol. Med. Rep.* *10*, 695–700.
- Richard, C.L., and Blay, J. (2007). Thiazolidinedione drugs down-regulate CXCR4 expression on human colorectal cancer cells in a peroxisome proliferator activated receptor gamma-dependent manner. *Int. J. Oncol.* *30*, 1215–1222.
- Rodeheffer, M.S., Birsoy, K., and Friedman, J.M. (2008). Identification of white adipocyte progenitor cells in vivo. *Cell* *135*, 240–249.
- Sengenès, C., Miranville, A., Maumus, M., de Barros, S., Busse, R., and Bouloumié, A. (2007). Chemotaxis and differentiation of human adipose tissue

- CD34+/CD31- progenitor cells: role of stromal derived factor-1 released by adipose tissue capillary endothelial cells. *Stem Cells* 25, 2269–2276.
- Shulman, G.I. (2000). Cellular mechanisms of insulin resistance. *J. Clin. Invest.* 106, 171–176.
- Shulman, G.I. (2014). Ectopic fat in insulin resistance, dyslipidemia, and cardiometabolic disease. *N. Engl. J. Med.* 371, 1131–1141.
- Soccio, R.E., Chen, E.R., and Lazar, M.A. (2014). Thiazolidinediones and the promise of insulin sensitization in type 2 diabetes. *Cell Metab.* 20, 573–591.
- Spalding, K.L., Arner, E., Westermark, P.O., Bernard, S., Buchholz, B.A., Bergmann, O., Blomqvist, L., Hoffstedt, J., Näslund, E., Britton, T., et al. (2008). Dynamics of fat cell turnover in humans. *Nature* 453, 783–787.
- Szendroedi, J., and Roden, M. (2009). Ectopic lipids and organ function. *Curr. Opin. Lipidol.* 20, 50–56.
- Taylor, R., and Holman, R.R. (2015). Normal weight individuals who develop type 2 diabetes: the personal fat threshold. *Clin. Sci. (Lond.)* 128, 405–410.
- Uezumi, A., Fukada, S., Yamamoto, N., Takeda, S., and Tsuchida, K. (2010). Mesenchymal progenitors distinct from satellite cells contribute to ectopic fat cell formation in skeletal muscle. *Nat. Cell Biol.* 12, 143–152.
- Virtue, S., and Vidal-Puig, A. (2008). It's not how fat you are, it's what you do with it that counts. *PLoS Biol.* 6, e237.
- Virtue, S., and Vidal-Puig, A. (2010). Adipose tissue expandability, lipotoxicity and the Metabolic Syndrome—an allostatic perspective. *Biochim. Biophys. Acta* 1801, 338–349.
- Wang, Q.A., Tao, C., Gupta, R.K., and Scherer, P.E. (2013). Tracking adipogenesis during white adipose tissue development, expansion and regeneration. *Nat. Med.* 19, 1338–1344.
- Yao, L., Heuser-Baker, J., Herlea-Pana, O., Zhang, N., Szweda, L.I., Griffin, T.M., and Barlic-Dicen, J. (2014). Deficiency in adipocyte chemokine receptor CXCR4 exacerbates obesity and compromises thermoregulatory responses of brown adipose tissue in a mouse model of diet-induced obesity. *FASEB J.* 28, 4534–4550.
- Zuk, P.A., Zhu, M., Ashjian, P., De Ugarte, D.A., Huang, J.I., Mizuno, H., Alfonso, Z.C., Fraser, J.K., Benhaim, P., and Hedrick, M.H. (2002). Human adipose tissue is a source of multipotent stem cells. *Mol. Biol. Cell* 13, 4279–4295.

STAR★METHODS

KEY RESOURCES TABLE

REAGENT or RESOURCE	SOURCE	IDENTIFIER
Antibodies		
Allophycocyanin (APC) Rat IgG2b, κ Isotype control (Clone 27-35)	BD biosciences	Cat# 555745; RRID:AB_398612
Allophycocyanin (APC) rat against mouse CXCR4 (Clone REA107)	Miltenyi Biotec	Cat#130-102-245; RRID:AB_2655759
Anti APC micro beads	Miltenyi Biotec	Cat# 130-090-855; RRID:AB_244367
Anti FITC micro beads	Miltenyi Biotec	Cat# 130-048-701; RRID:AB_244371
Brilliant Violet 421 Rat IgG2b, κ Isotype Ctrl (Clone RTK4530)	Biolegend	Cat# 400639; RRID:AB_10895758
Chicken anti-rat Alexa 647	ThermoFisher	Cat# A21472; RRID:AB_2535875
Fluorescein isothiocyanate (FITC) rat against mouse CD31 (Clone 390)	Miltenyi Biotec	Cat# 130-102-519; RRID:AB_2657307
Fluorescein isothiocyanate (FITC) rat against mouse CD4 (Clone GK1.5)	BD biosciences	Cat# 553729; RRID:AB_395013
Fluorescein isothiocyanate (FITC) rat against mouse CD45 (Clone 30-F11)	Miltenyi Biotec	Cat# 130-102-491; RRID:AB_2659919
Goat anti-hamster Alexa 546	ThermoFisher	Cat# A21111; RRID:AB_2535760
Hamster PerCP/Cy5.5 against mouse CD3 ϵ	Biolegend	Cat# 100327; RRID:AB_893320
Pacific blue rat IgG2b Isotype control (Clone RTK4530)	Biolegend	Cat# 400627; RRID:AB_493561
PerCP/Cy5.5 Armenian Hamster IgG Isotype Control (Clone HTK888)	Biolegend	Cat# 400931; RRID:AB_2797557
Purified Rat Anti-Mouse CD16/CD32 (Mouse BD Fc Block)	BD biosciences	Cat# 553141; RRID:AB_394656
Rabbit monoclonal against mouse pan Akt	Cell signaling technology	Cat# 4691; RRID:AB_915783
Rabbit polyclonal (Ser473) against mouse phospho-Akt	Cell signaling technology	Cat# 9271; RRID:AB_329825
Rabbit polyclonal against GFP	ProteinTech Europe	Cat# 50430-2-AP; RRID:AB_11042881
Rat Allophycocyanin (APC) against mouse CD19 (Clone 1D3)	BD biosciences	Cat# 550992; RRID:AB_398483
Rat Allophycocyanin (APC) against mouse CD45 (Clone 30-F11)	BD biosciences	Cat#559864; RRID:AB_398672
Rat Brilliant Violet 421 against mouse CXCR4 (Clone L276F12)	Biolegend	Cat# 146511; RRID:AB_2562788
Rat monoclonal against CD31 (Clone MEC13.3)	BD biosciences	Cat#BD550274; RRID:AB_393571
Rat monoclonal against CD45 (Clone 30-F11)	Santa cruz biotechnology	Cat# sc-53665; RRID:AB_629093
Rabbit monoclonal against CXCR4	ThermoFisher Scientific	Cat#PA3-305; RRID:AB_2091817
Rat monoclonal against Sca1 (D6)	BD biosciences	Cat#557403; RRID:AB_396686
Rat Pacific blue against mouse F4/80 (Clone A3-1)	Biorad	Cat# MCA497PB; RRID:AB_567114
Rat phycoerythrin (PE)-cyanin7 against mouse CD45 (Clone 30-F11)	BD biosciences	Cat# 552848; RRID:AB_394489
Rat R-phycoerythrin (PE) against mouse CD31 (Clone MEC13.3)	BD biosciences	Cat# 553373; RRID:AB_394819
Rat R-phycoerythrin (PE) against mouse CD8b (Clone H35-17.2)	BD biosciences	Cat# 550798; RRID:AB_393887
Rat V500 against mouse Ly6AE/Sca-1 (Clone D7)	BD biosciences	Cat# 561228; RRID:AB_10584334
R-phycoerythrin (PE) Rat IgG2a, κ Isotype Control (Clone R35-95)	BD biosciences	Cat# 553930; RRID:AB_479719
Syrian Hamster monoclonal [RTD4E10] against podoplanin, gp36	Abcam	Cat# Ab11936; RRID:AB_298717
Chemicals, Peptides, and Recombinant Proteins		
[2-3H]deoxyglucose	PerkinElmer	Cat#NET328A250UC
3,3',5-Triiodo-L-thyronine	Sigma Aldrich	Cat# T6397
AMD3100, Plerixafor hydrochloride	Interchim	Cat# 10011332
BODIPY 558/568 C12 (dodecanoic acid)	ThermoFisher Scientific	Cat# D3835
BODIPY 493/503	Invitrogen	Cat#03922
Cell culture insert	Falcon	Cat# 35/3093
Clarity	Biorad	Cat# 1705061

(Continued on next page)

Continued		
REAGENT or RESOURCE	SOURCE	IDENTIFIER
Collagenase NB4	Coger	Cat# SER-1745401
cOmplete, Mini, EDTA-free Protease Inhibitor Cocktail	Roche	Cat# 4693159001
Cortisol	Sigma Aldrich	Cat# C106
Dispase II	Roche	Cat# 04942078001
DNase I from bovine pancreas	Sigma Aldrich	Cat# 11284932001
Horse serum	Sigma Aldrich	Cat# 1138
Human (rDNA) Insulin Humulin R U-100	Eli Lilly	Cat# HI-213
Laemmli buffer	Sigma Aldrich	Cat# 38733
MACS flow buffer	Miltenyi Biotec	Cat# 130.091.221
NCS	Sigma Aldrich	Cat# N4637
PhosSTOP, phosphatase inhibitor cocktail	Roche	Cat# 4906837001
Pioglitazone hydrochloride	Sigma Aldrich	Cat# E6910
PolyVynilbifluorid membranes	Amersham	Cat# GE10600100
Qiazol	QIAGEN	Cat# 79306
RIPA lysis buffer	Sigma Aldrich	Cat# 20-188
Tamoxifen	Sigma Aldrich	Cat# T5648-5G
TRIzol	Thermofisher Scientific	Cat# A33251
Critical Commercial Assays		
Agencourt RNA Clean kit	Agencourt	Cat# NC0068576
CLICK PLUS EDU 488 FLOW KIT	Life technologies	Cat# C10633
Encore® Biotin Module kit	NuGEN	Cat# 4200
Experion RNA Stdsens analysis kit	Biorad	Cat# 7007103
High-Capacity cDNA Reverse Transcription Kit	Applied Biosystems	Cat# 4368814
Mouse CXCL12/SDF-1 alpha Quantikine ELISA Kit	Biotechne R&D	Cat# MCX120
Mouse Gene 1.1 ST Array Strip Affymetrix	Thermofisher Scientific	Cat# 901628
Mouse insulin Elisa kit	Alpco	Cat# 80-INSMS-E01
Ovation® PicoSL WTA System	NuGEN	Cat# 3302
Power SYBR Green PCR Mater Mix	Applied Biosystems	Cat# 4367659
Rneasy kit	QIAGEN	Cat# 217004
Deposited Data		
Microarray data of ASCs isolated from murine ScAT and PGAT	NCBI Gene Expression Omnibus (GEO)	GEO: GSE127928
Experimental Models: Organisms/Strains		
Mouse: C57BL/6J	Janvier	Cat# SC-C57J-M
Mouse: Tg(Cd34-EGFP)MF6Gsat/Mmcd	MMRRC (Mutant Mouse Regional Resource Center)	Cat# 032848-UCD
Mouse: B6.Cg-Gt(ROSA)26Sortm6(CAG-ZsGreen1)Hze/J	Jackson laboratories	Cat# 7906
Mouse: C57BL/6J-Tg(Adipoq-cre/ERT2)1Soff/J	Jackson laboratories	Cat# 025124
Normal chow diet 10%kcal fat	Research Diets	Cat# D12450B
High fat diet 45%kcal fat	Research Diets	Cat# D12451
Oligonucleotides		
Primers for qPCR, see Table S1	This paper	N/A
Software and Algorithms		
Affymetrix GeneChip Command Console (AGCC) Software		https://www.thermofisher.com
BD FACSDiva software		http://www.bdbiosciences.com
ChemiDoc XRS+ System		http://www.bio-rad.com
EchoMRI		https://www.caymanchem.com/home
GeneAmp7500		https://www.thermofisher.com

(Continued on next page)

Continued

REAGENT or RESOURCE	SOURCE	IDENTIFIER
GeneAtlas™ System		http://www.thermofisher.com
Graphpad Prism 5		https://graphpad.com
ImageJ		https://imagej.nih.gov/ij
Imaris		http://www.bitplane.com
Incucyte S3 software		https://www.essenbioscience.com/en/
Ingenuity Pathway Analysis version 7.6		https://www.qiagenbioinformatics.com
Kalusa		https://www.beckman.com
Operetta High-Content Imaging System		http://www.perkinelmer.com
Partek Genomic Suite™ software version 6.4		http://www.partek.com
Zen Imagin Software		https://www.zeiss.com/corporate/int/home.html

CONTACT FOR REAGENT AND RESOURCE SHARING

Further information and requests for resources and reagents should be directed to and will be fulfilled by the Lead Contact, Coralie Sengenès (coralie.sengenès@inserm.fr).

EXPERIMENTAL MODEL AND SUBJECT DETAILS

Eight-week-old male C57BL/6J mice (Janvier); Tg(Cd34-EGFP)MF6Gsat/Mmcd mice, called CD34-GFP (MMRRC); B6.Cg-Gt (ROSA)26Sortm6(CAG-ZsGreen1)Hze/J mice, called ZsGreen (both Jackson Laboratories); and C57BL/6J-Tg(Adipoq-cre/ERT2)1Soff/J mice, called Adiponectin-Cre (Jackson Laboratories) were kept under controlled light (12-hr light/dark cycles) and temperature (22°C–24°C). All studies were carried out under the INSERM Animal Care Facility guidelines and local ethical approval from Toulouse Ranguel Hospital. Mice were fed a standard diet (ND; 10% kcal fat; Research Diets D12450B) or high fat diet (HFD; 45% kcal fat; Research Diets D12451). Food intake was monitored weekly. Body mass composition was evaluated by a quantitative nuclear magnetic resonance system (EchoMRI 3-in-1, Echo Medical Systems).

METHOD DETAILS**Animal treatments**

A group of C57BL/6J mice was treated weekly with the CXCR4 antagonist AMD3100 (5 mg/kg, i.p.; Interchim) or saline solution (NaCl 0.9%) or with pioglitazone (10 mg/kg, i.p.; Sigma-Aldrich) for up to 8 weeks. In some cohorts, 1 week before sacrifice, an intraperitoneal glucose tolerance test was performed. Mice were fasted for a few hours, then injected intraperitoneally with 1 g/kg lean mass of D-glucose. Blood glucose levels were monitored from the tip of the tail with a glucometer (Accucheck, Roche) at 0, 15, 30 and 60 min after injection. Supplemental blood sampling was performed at 15 min for insulin measurement. At the end of the protocol, animals were sacrificed, and blood and bone marrow (BM) were collected. Subcutaneous (Sc), perigonadic (PG), mesenteric (Mes), perirenal (PR), pericardiac and periaortic ATs, quadriceps, soleus, EDL, heart, liver, kidney, lungs and spleen were dissected. For insulin signaling experiments, soleus muscles were incubated at 37°C for 20 min in Krebs-Henseleit buffer with 100 nM insulin (Badin et al., 2013), then freeze-clamped in liquid nitrogen and stored at –80°C. For the insulin tolerance test and tissue-specific [2-³H] deoxyglucose uptake, mice from a dedicated cohort were fasted for a few hours, then injected intraperitoneally with a bolus of insulin (3 units/kg) and [2-³H]deoxyglucose (4 μCi/kg; PerkinElmer). Blood glucose levels were monitored as described above at 0, 15 and 30 min after injection. Animals were decapitated and blood was collected. Organs and tissues were rapidly excised, weighed and snap-frozen in liquid nitrogen before being stored at –80°C. The muscle-specific clearance index (Rg) was determined as described (Laurens and Moro, 2016).

For ScAT grafting experiments, C57BL/6J mice were anesthetized with isoflurane, skin was surgically incised and a 10-mg piece of ScAT from CD34-GFP or ZsGreen mice was inserted into the ScAT of non-fluorescent recipient mice before skin was stitched, a technique routinely performed in the lab. Two weeks after surgery, animals were challenged by a diet and/or pharmacologically treated for 8 weeks. With the ZsGreen SCAT graft, after 8 weeks of HFD, animals were treated with tamoxifen (50 mg/kg) i.p. for 5 consecutive days before cre recombination. Mice underwent a washout period of 10 days before sacrifice.

Isolation of the Stroma Vascular Fraction (SVF) from AT and BM and quadriceps muscle

Sc, Mes, and PG ATs were minced and digested with collagenase (NB4, Coger), (250 U/mL in phosphate-buffered saline [PBS], 2% bovine serum albumin [BSA], pH 7.4) for 30 to 60 min at 37°C under constant agitation. For BM SVF isolation, femurs were flushed

with PBS. After centrifugation (300 g, 10 min, room temperature [RT]), the floating mature adipocytes were removed and the pellet containing the SVF was briefly suspended in erythrocyte lysis buffer (ELB; 155 mmol/L NH_4Cl ; 5.7 mmol/L K_2HPO_4 ; 0.1 mmol/L EDTA, pH $\frac{1}{4}$ 7.3) at RT. Freshly harvested muscles were minced and digested with collagenase B (0.5 U/ml, Roche) and dispase II (2.4 U/ml, Roche) in Hank's balanced Saline Solution (HBSS) + 2.5 mM Ca^{2+} for two rounds of 30 min at 37°C under agitation, separated by mechanical dissociation with 10 passages through a G18 needle. The reaction was stopped by adding a large volume of α MEM+10% newborn calf serum (NCS), then samples were filtered, 34 μm , and centrifuged (300 g, 10 min) to eliminate the supernatant. After filtration through a 34- μm sieve, SVF cells from AT, BM or muscle were resuspended in flow cytometry (FACS) buffer (PBS; 2 mmol/L EDTA; 0.5% BSA) for flow cytometry analyses or stored at -20°C for RNA isolation.

Adipose Stem Cell (ASC) Sorting, Adipogenic Differentiation and Transwell Migration Assay

Murine crude AT-derived SVF was depleted in CD45⁺ and CD31⁺ cells by using mouse FICT-CD45 and FITC-CD31 microbeads and the autoMACS Pro Separator (MACS Cell Separation, Miltenyi Biotec SAS) according to the manufacturer's instructions (CD45⁺ and CD31⁺ cell fraction purity was 99.5% \pm 0.2% and 99.2% \pm 0.2%, n = 8). For further CXCR4-ASC isolation, positive sorting involved using mouse CXCR4-APC microbeads (CXCR4⁺ cell fraction purity was > 90%). For adipogenic differentiation, total SVF or ASCs were plated at 80,000 cells per cm^2 in α MEM supplemented with 10% NCS. After 24 hr at 37°C and 5% CO_2 , cells were induced to undergo adipogenic differentiation with α MEM supplemented with 2% NCS, 66 nmol/L insulin, 1 nmol/L triiodothyronine, and 100 nmol/L cortisol. After 7 days of culture, cells were imaged by using a Nikon Eclipse TE2000-S microscope.

For cell migration assays, ASCs were plated in fibronectin pre-coated 8- μm pore inserts (Falcon) at 80,000 cells per cm^2 in α MEM supplemented with 0.1% NCS and without or with 100 μM pioglitazone. Inserts were immersed in α MEM supplemented with 0.1% or 10% NCS for 24 hr for attracting migratory factors. Medium in the bottom well containing the migrating ASCs was collected and the bottom was trypsinized. Cells were then counted by flow cytometry (LSR Fortessa and FACSDiva, BD Biosciences) over a fixed time period. For Incucyte kinetics experiments, ASC isolated from ScAT of C57BL/6J mice were plated at 2000 cells per well in a 96-well plate loaded with 100 μl plasma obtained from animals fed an ND or HFD and treated or not with pioglitazone. Real-time kinetics data were obtained over 40 hr and analyzed by using Incucyte S3 software (Essenbioscience).

Flow Cytometry

Isolated cells from ATs, BM or muscle were incubated (25 in, 4°C, dark) with phycoerythrin (PE)-CD31 or -CD8b; allophycocyanin (APC)-CD45, -CD31 or -CD19; fluorescein isothiocyanate (FITC)-CD4; Pacific blue-F4/80, PerCP-Cy5.5-CD3e, Sca-1-V500 (BD Biosciences), Brilliant violet (BV) 421-CXCR4 antibodies or the appropriate isotype controls (BD Biosciences). After washing, the labeled cells were quantified on an LSR Fortessa flow cytometer and analyzed by using FACSDiva (BD Biosciences).

Proliferation assay

Proliferation *in vivo* was assessed with the Click Plus EdU 488 Flow Kit (Life Technologies) following the manufacturer's instructions. Briefly, animals were injected twice with Edu (40 $\mu\text{g/g}$) at 48 and 24 hr before sacrifice. SVF isolation from different tissues was as described. Isolated SVF-derived cells were fixed and permeabilized and further incubated for 1 hr at 37°C with a Click It reaction cocktail to reveal Edu staining with Alexa Fluor 488 in proliferative cells.

Adipose Tissue Immunohistochemistry

AT depots and quadriceps muscle were fixed in neutral buffered 4% (w/v) paraformaldehyde (24 hr, RT) and embedded in 2% agarose gel, and 300- μm slices were obtained by using a vibroslice (Campden Instruments). Tissue slices were blocked in PBS/0.2% triton/2% horse serum (30 min, RT) and incubated in PBS/0.2% triton/2% horse serum with primary antibodies overnight at 4°C [anti-podoplanin (hamster, 1:150, Abcam), anti-CD45 (rat, 1:200, Santa Cruz Biotechnology), anti-CD31 (rat, 1:150, BD Biosciences), anti-CXCR4 (rabbit, 1:150, Thermo Fisher Scientific), anti-Sca1 (rat, 1:150, BD Biosciences)]. After washing steps in PBS/0.2% triton, AT samples were incubated overnight with secondary antibodies [anti-hamster (Alexa fluor 546, 1:200, Molecular Probes), anti-rat (Alexa fluor 647, 1:200, Molecular Probes), anti-rabbit (Alexa fluor 657, 1:200, Molecular Probes)]. Nuclei were stained with DAPI (1:10000, Invitrogen). Fluorescence was analyzed under a Zeiss LSM780 confocal microscope (Genotoul Platform, Toulouse, France, <http://trigenotoul.com/en/>). For ectopic adipocyte quantification in quadriceps muscle, slices were incubated for 2 hr, RT with Dodeca Bodipy (Thermo Fisher Scientific) 1:2000 or BODIPY 493/503 (Invitrogen) 1:500 in PBS/0.2% triton and nuclei were stained with DAPI (1:10000, Invitrogen). Imaging and fluorescence quantification were performed on entire muscle sections with the Operetta High-Content Imaging System (Perkin Elmer).

RNA Isolation and Real-Time RT-PCR Analysis

Total RNA was extracted from murine AT and SVF-derived ASCs by using the RNeasy kit (QIAGEN). RNA concentrations were determined by using Nanodrop (Thermo Fisher Scientific). Reverse transcription involved 0.5 μg of RNA by using Superscript II, random hexamers, and dNTPs according to the manufacturer's instructions (Invitrogen). The primer for CXCR4 was provided by Applied Biosystems (Assays on demand: Mm01292123-m1). Amplification reaction was carried out with 10 ng complementary DNA samples in 96-well plates (Applied Biosystems) in a GeneAmp 7500 sequence detection system. The PCR mixture contained 1.5 μL of 2 μM primers and 5 μL of 2 Fast SybrGreen PCR master Mix (Applied Biosystems). All reactions were performed at 50°C (2 min), 95°C

(10 min), then 40 cycles of 95°C (15 s) and 60°C (1 min). The results were analyzed by use of GeneAmp 7500, and all values were normalized to 18 s and 36B4 RNA levels.

Microarray Transcriptome Hybridization and Analysis

After extraction with TRIzol reagent (Invitrogen; RNAs were controlled by using the Nanodrop ND-200 and Experion RNA StdSens analysis kit (Biorad). The Ovation PicoSL WTA System (NuGEN) was used for cDNA synthesis and amplification. An amount of 25 ng total RNA was reverse transcribed with a primer mix containing both polyT and random sequences for whole transcriptome coverage, followed by second-strand cDNA synthesis with Ribo-Single Primer Isothermal Amplification (SPIA) technology (for detailed methods: <https://www.nugen.com/technology/spia>). The amplified SPIA cDNA was further purified with Agencourt RNA Clean Beads. An amount of 2.5 µg SPIA cDNA was then fragmented and labeled by using the Encore Biotin Module (NuGEN) and hybridized to a mouse gene chip (Mo Gene 1.1 ST Array Strip; Affymetrix). Array hybridization, washing and staining were performed as described by the manufacturer (GeneAtlas Hybridization, Wash and Stain Kit for WT Array Strips; Affymetrix) with the GeneAtlas System. Arrays were then scanned (GeneAtlas Imaging Station; Affymetrix) and analyzed by using Command Console. CEL files were imported into Partek Genomic Suite v6.4 (Partek, Inc., MO, USA) for normalization and expression comparison. Genes with expression at ≥ 1.5 -fold difference between ScAT and perigonadal (PG) AT (PGAT) originating from ASCs and $p < 0.05$. Cluster analyses and principal component analysis were conducted with Partek default settings. Gene networks representing key genes were identified by using Ingenuity Pathways Analysis v7.6 (IPA; Ingenuity Systems).

Protein Extraction and Western Blot and ELISA Analysis

For ELISA, proteins were extracted from mouse soleus and quadriceps muscles and AT. Tissues were homogenized in ice-cold RIPA buffer supplemented with complete protease inhibitor tablets (Roche Diagnostics, Basel, Switzerland) and phosphatase inhibitor tablets (PhosSTOP, SigmaAldrich) with the TissueLyser Bead Homogenizer (QIAGEN). Protein extracts or undiluted plasma was analyzed according to the manufacturer's instructions (Quantikine ELISA mouse CXCL12, Bio-technie, Minneapolis, MN). Results were normalized per gram tissue or total protein content.

For western blot analysis, soleus muscle was homogenized and protein underwent western blot analysis as described (Badin et al., 2013). Briefly, 30 µg solubilized protein was run on 4% to 20% gradient SDS-PAGE (Bio-Rad, Hercules, CA), transferred to nitrocellulose membrane (Hybond ECL; Amersham Biosciences), and incubated with the primary antibodies for phospho-Akt (Ser473) or total Akt (1:1000 final dilution, Cell Signaling Technology) overnight at 4°C. After washing, an appropriate secondary antibody (anti-rabbit IgG peroxidase conjugated) was applied for 1 hr at 1:10000. Blots were washed, incubated in commercial enhanced chemiluminescence reagents (Bio-Rad) and analyzed with Chemidoc XRS (Bio-Rad). To prove equal loading of samples, blots were re-incubated with anti-GAPDH antibody (1:5000 final dilution, Cell Signaling Technology).

QUANTIFICATION AND STATISTICAL ANALYSIS

Data are expressed as mean \pm SEM. Graphic representation of data as well as all statistical tests were performed with GraphPad Prism (San Diego, CA). Comparisons among different groups were analyzed by one-way ANOVA, then post hoc Dunn and multiple comparison tests, Mann-Whitney U test or two-way ANOVA and Bonferroni post-tests. Simple linear regressions were performed with Pearson's test. The number of independent experiments and n values are specified in the figure legends. Differences were considered statistically significant at $p \leq 0.05$.

DATA AND SOFTWARE AVAILABILITY

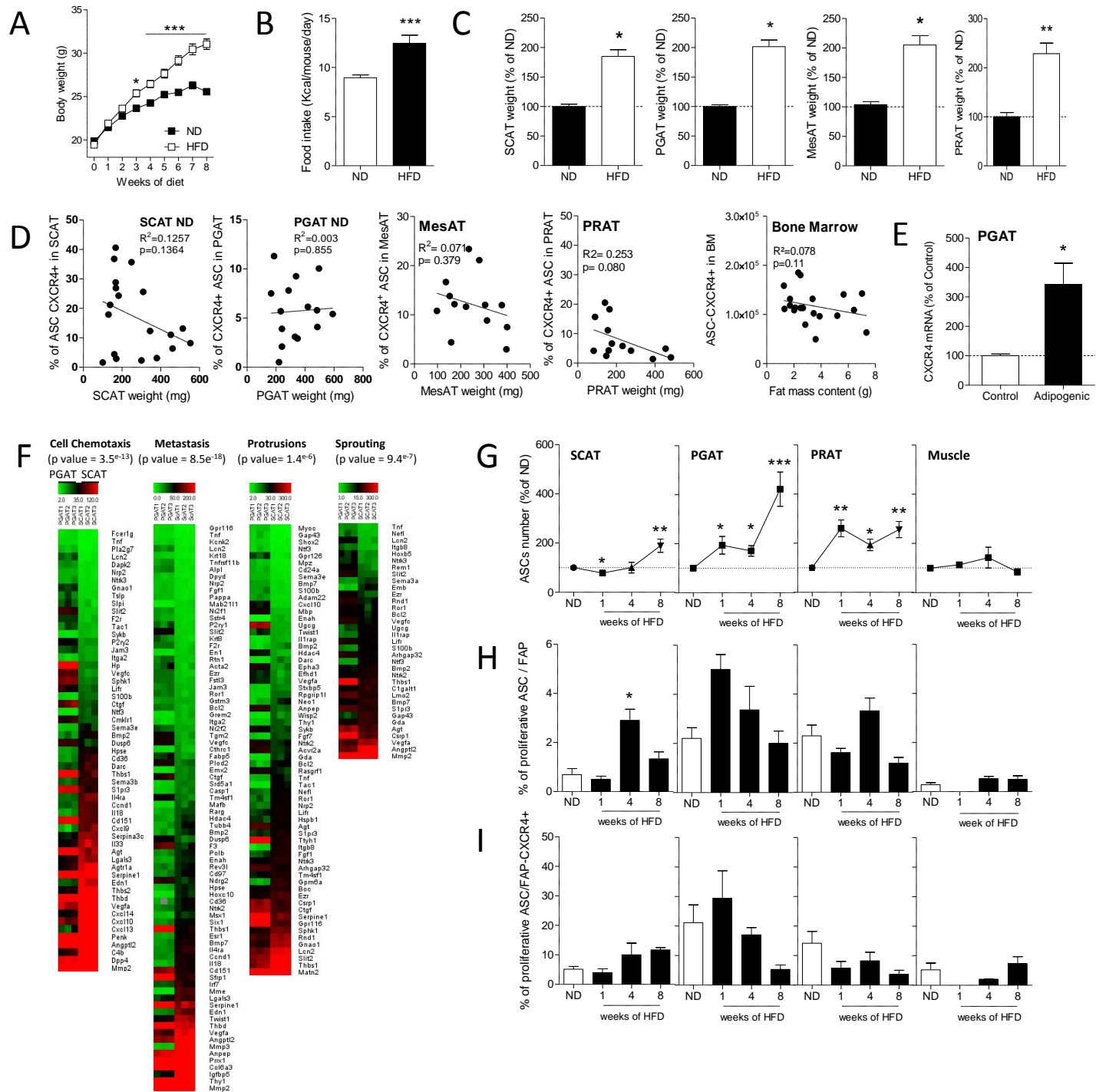
Microarray data of ASCs isolated from murine ScAT and PGAT reported in this paper has been deposited to NCBI Gene Expression Omnibus (GEO), GEO: GSE127928.

Cell Reports, Volume 27

Supplemental Information

The Release of Adipose Stromal Cells from Subcutaneous Adipose Tissue Regulates Ectopic Intramuscular Adipocyte Deposition

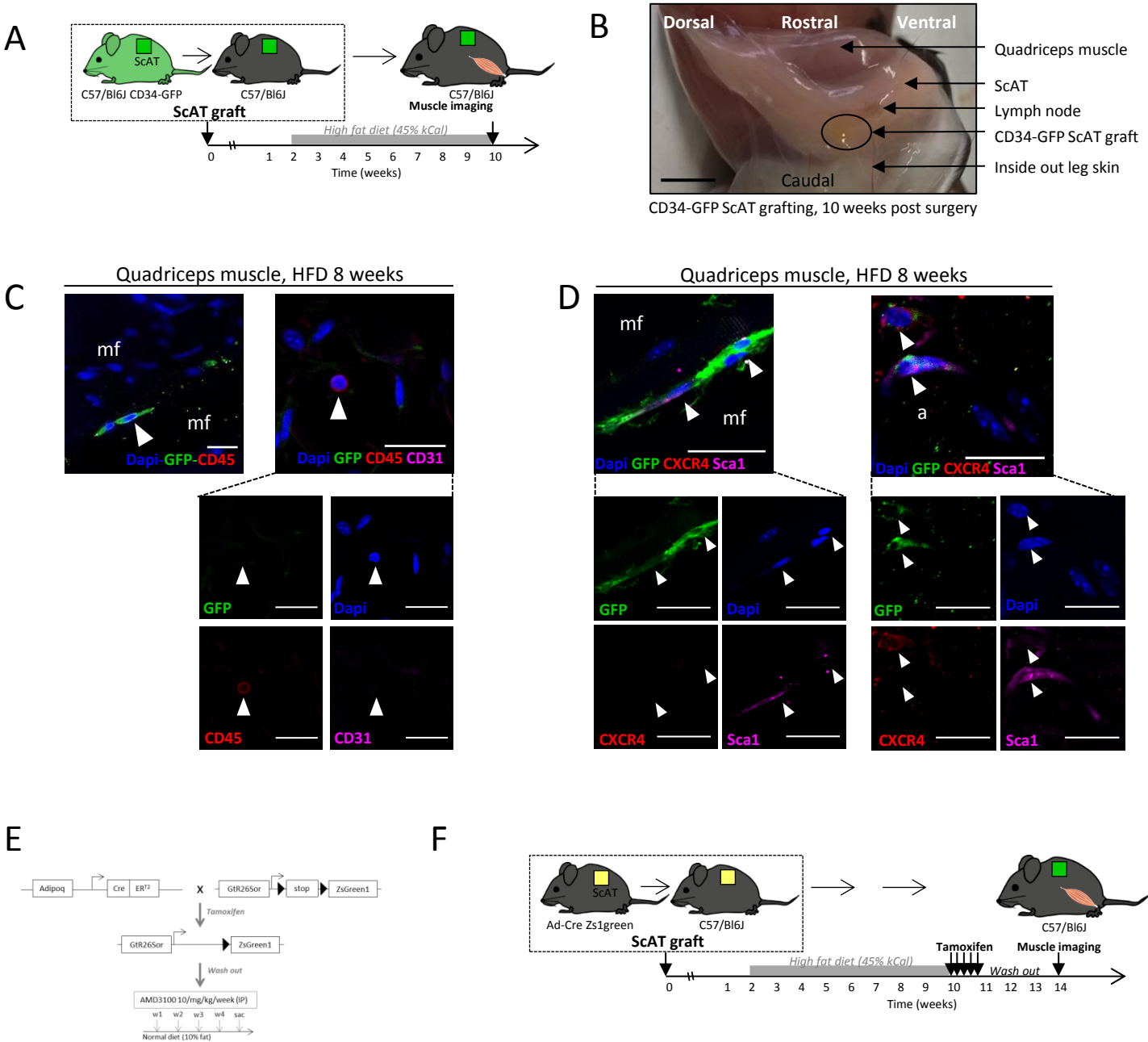
Amandine Girousse, Marta Gil-Ortega, Virginie Bourlier, Célia Bergeaud, Quentin Sastourné-Arrey, Cédric Moro, Corinne Barreau, Christophe Guissard, Julie Vion, Emmanuelle Arnaud, Jean-Philippe Pradère, Noémie Juin, Louis Casteilla, and Coralie Sengenès



Supplemental figure 1: **High-fat diet specifically induces the mobilization of CXCR4⁺-ASCs from ScAT towards skeletal muscle.** Related to Figure 1.

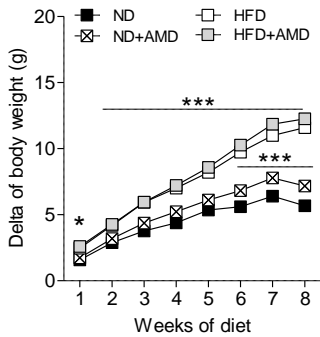
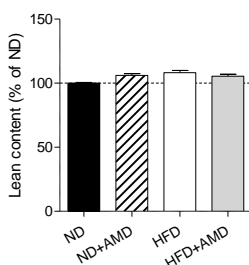
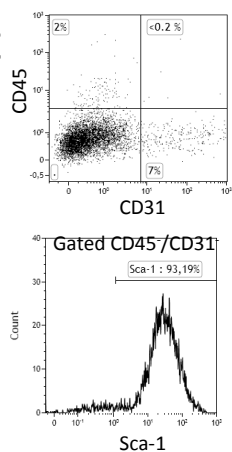
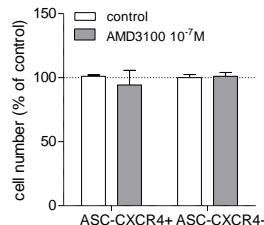
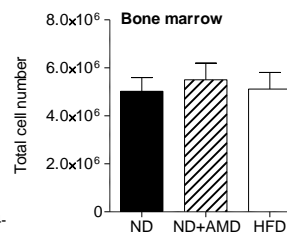
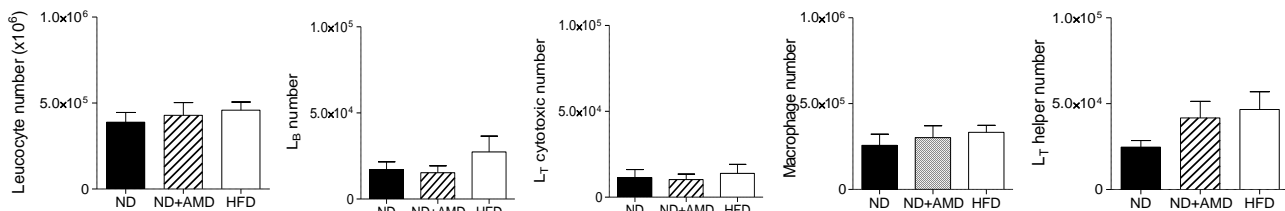
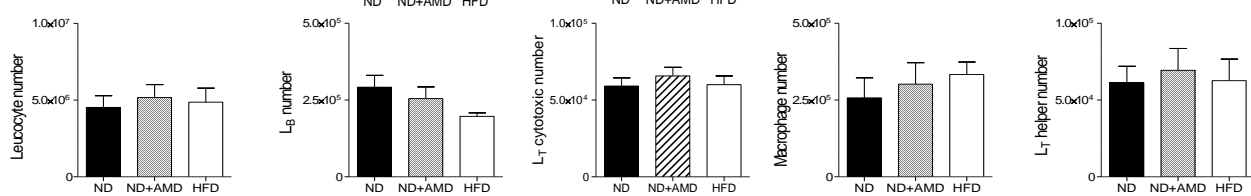
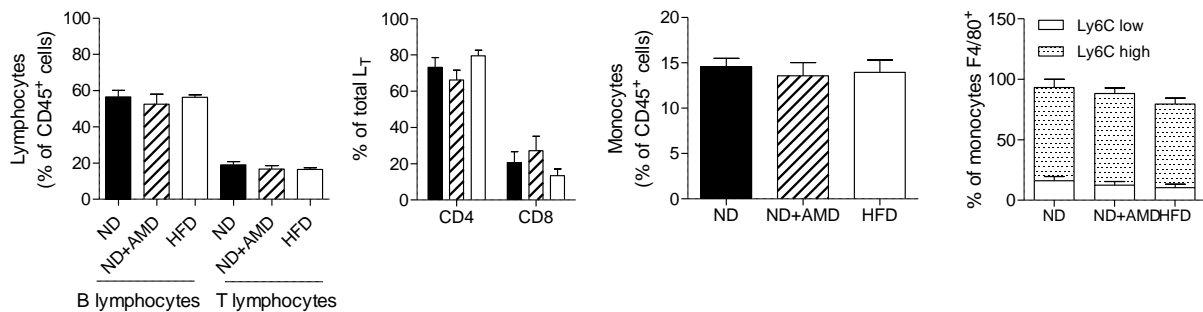
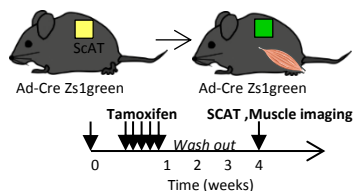
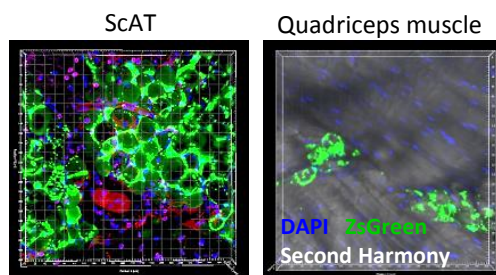
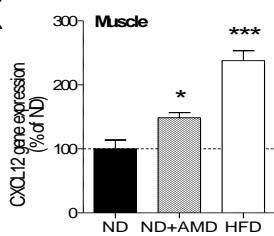
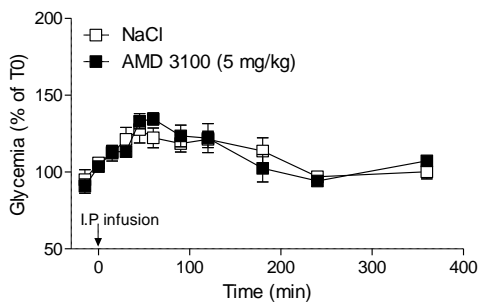
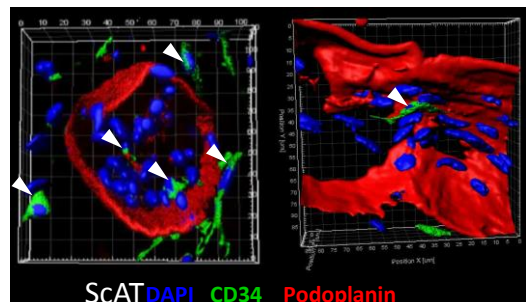
Mice were fed a normal diet (ND) or high-fat diet (HFD) for 8 weeks.

(A) Body weight curve. (B) Food intake. (C) Weight of adipose tissue (AT; from the left, subcutaneous [ScAT], perigonadal [PGAT], mesenteric [MesAT] and perirenal AT [PRAT]). (D) Simple linear regression between percentage of CXCR4-expressing ASCs in stroma vascular fraction isolated from ScAT, PGAT, MesAT, PRAT and bone marrow and tissue weight (or animal weight in case of BM). R² and p values are presented on the graphs. (E) Cxcr4 mRNA expression of ASCs isolated from PGAT and cultivated in normal medium or after 7 days in pro-adipogenic media. (F) Heat maps of differentially regulated pathways in ASCs isolated from ScAT and PGAT. (G) Time course of ASC number in ScAT, PGAT, PRAT and muscle. (H-I) Time course of proliferative ASCs (H) and CXCR4-expressing ASCs (I). (A-E) n = 5 to 18; data are mean ± SEM; one-way ANOVA Dunn's post-test; * p ≤ 0.05, ** p ≤ 0.01, *** p ≤ 0.001 compared to ND or control condition.



Supplemental figure 2: ScAT grafting strategies for observing muscular HFD-mediated cellular events originating from ScAT. Related to Figures 1 and 2

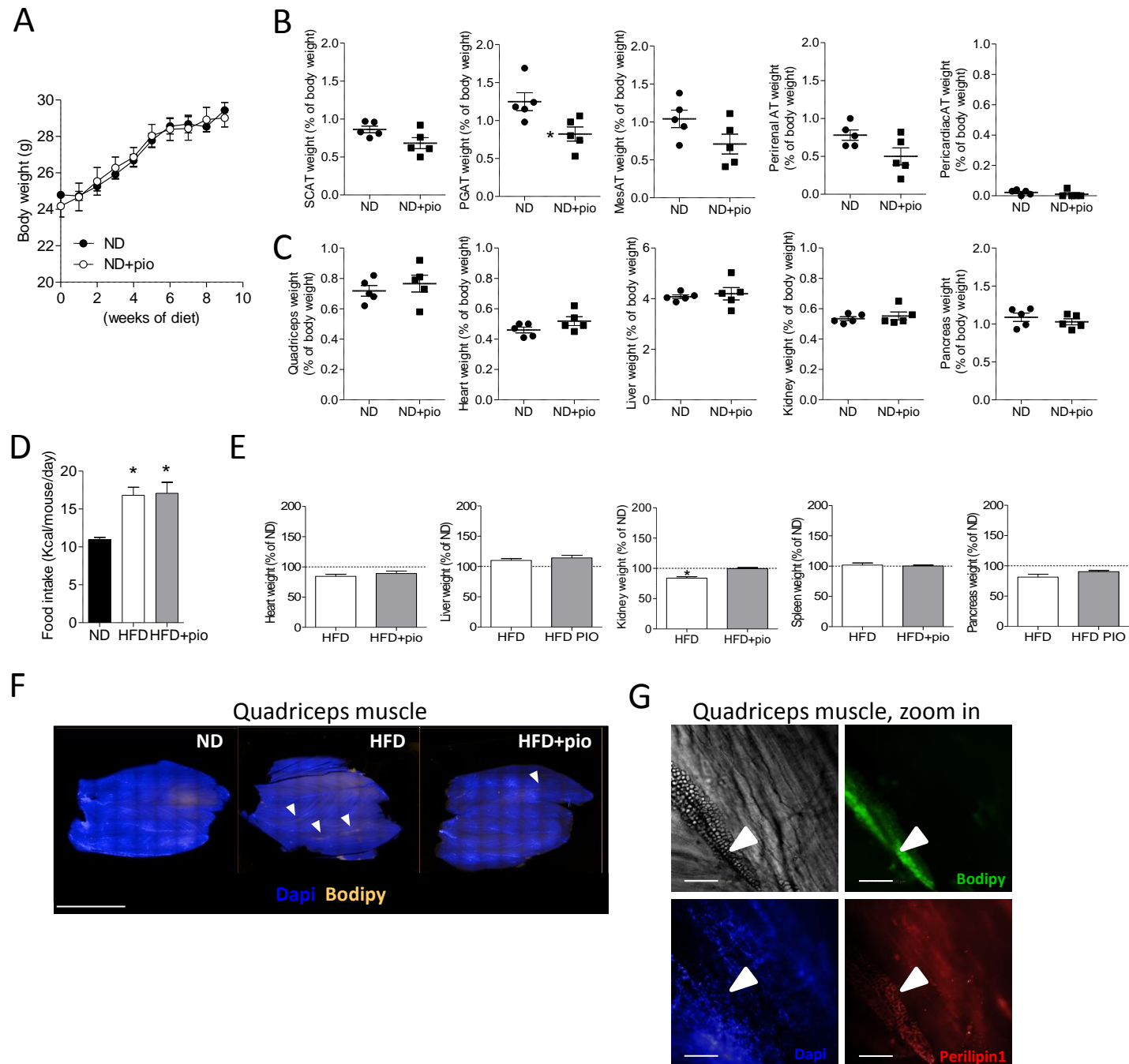
(A) Experimental design of the CD34-GFP fat graft pad experiment. (B) Picture of ScAT 10 weeks after CD34-GFP ScAT graft surgery. Scale bar, 1 cm. (C-D) Confocal immunofluorescence image of a representative quadriceps muscle section of two HFD-fed animals. Agarose-embedded sections are immunostained with antibodies recognizing GFP and CD45. Arrowheads point to ASCs. Scale bar, 20 μ m. (E) Schematic representation of the adiponectin-ZsGreen mouse breeding and protocol of AMD3100 treatment. (F) Zs1Green ScAT graft experimental protocol scheme.

A**B****C****D****E****F****ScAT****G****Bone Marrow****H****Blood****I****J****K****L****M**

Supplemental figure 3: **AMD3100 treatment promotes ectopic fat deposition impairing glucose tolerance.** Related to figure 3.

Mice were fed with an ND or HFD for 8 weeks, then injected weekly with vehicle NaCl 0.9% or AMD3100.

(A) Body weight curve. (B) Lean mass measurement. (C) Representative flow cytometry dot plot of ASCs isolated from ScAT with the immunophenotype CD45⁻/CD31⁻/Sca1⁺. (D) Cell proliferation assay in sorted ASCs from ScAT. (E) Total cell number in bone marrow. (F-G) Quantified flow cytometry of immune cell panels from stroma vascular fraction of ScAT (F) and bone marrow (G). From left, leucocytes (CD45⁺ cells), B lymphocytes (CD45⁺/CD3⁺/CD19⁺ cells), cytotoxic T lymphocytes (CD45⁺/CD3⁺/CD8⁺ cells), macrophages (CD45⁺/CD31⁺/F4/80⁺ cells) and helper T lymphocytes (CD45⁺/CD3⁺/CD4⁺ cells). (H) Quantified flow cytometry of immune cells in blood. From left, lymphocytes, % of T lymphocytes, monocytes and % of Ly6C monocytes populations. (I-J) Experimental protocol scheme and confocal immunofluorescence image of a representative quadriceps muscle section of two Zs1Green animals treated with AMD3100. Square unit 10 μ m. (K) Cxcl12 mRNA expression in quadriceps muscle after 8 weeks of protocol. (L) Blood glucose level after acute intraperitoneal injection of AMD3100 or NaCl. (M) Confocal immunofluorescence images of CD34-expressing ASCs (arrowheads) lying around or in lymphatic vessels of ScAT. Agarose-embedded sections were immunostained with antibodies recognizing podoplanin; surfacing of images was performed with Imaris software. White arrows show ASCs. Square unit 10 μ m (left) and 5 μ m (right). (A-B, E-H) n= 13 to 16, (C-D) n=3, (K-L) n=5-7; data are mean \pm SEM. One-way ANOVA Dunn's post-test; * p \leq 0.05, ** p \leq 0.01, *** p \leq 0.001 compared to ND or control condition.



Supplemental figure 4: **Pioglitazone treatment reduced HFD-mediated ectopic lipid deposition in vivo.** Related to Figure 4.

Mice were fed an ND or HFD for 8 weeks, then injected weekly with DMSO vehicle or pioglitazone.

(A) Body weight curve. (B) AT weight (from left, subcutaneous, perigonadal, mesenteric, peri-renal and peri-cardiac AT). (C) Non-AT weight (from left, quadriceps muscle, heart, liver, kidney and pancreas). (D) Food intake. (E) Non-AT weight (from left, heart, liver, kidney, spleen and pancreas). Dotted lines represent ND-fed animals. (F)

Immunofluorescence image of total quadriceps muscle section stained with Bodipy. White arrowheads point to clusters of adipocytes. Scale bar, 5 mm. (G) Zoom in of immunofluorescence image of total quadriceps muscle section stained with Bodipy and perilipin 1. White arrowheads point to clusters of adipocytes. Scale bar, 200 μ m. (A-E) $n = 5$ to 8; data are mean \pm SEM. Student's t test and one-way ANOVA Dunn's post-test; * $p \leq 0.05$, ** $p \leq 0.01$, *** $p \leq 0.001$ compared to ND or control condition.

Gene	Primer	Sequence (5' - 3')
<i>18s</i>	Forward	AGTCCCTGCCCTTTGTACACA
<i>18s</i>	Reverse	CGATCCGAGGGCCTCACTA
<i>36b4</i>	Forward	AGTCGGAGGAATCAGATGAGGAT
<i>36b4</i>	Reverse	GGCTGACTTGGTTGCTTTGG
<i>aP2</i>	Forward	TCACCATCCGGTCAGAGAGTA
<i>aP2</i>	Reverse	GCCATCTAGGGTTATGATGCTC
<i>CXCL12</i>	Forward	CCAAGGTCGTCGCCGTGCTG
<i>CXCL12</i>	Reverse	CTCGAAGAACCGGCAGGGGC
<i>CXCR4</i>	Forward	GCTCCGGTAACCACCACGGC
<i>CXCR4</i>	Reverse	TCCCGGAAGCAGGGTTCCTTGT
<i>cycloA</i>	Forward	GATGAGAACTTCATCCTAAAGCATACA
<i>cycloA</i>	Reverse	TCAGTCTTGGCAGTGCAGATAAA
<i>HPRT</i>	Forward	CTGGTGAAAAGGACCTCTCG
<i>HPRT</i>	Reverse	TGAAGTACTCATTATAGTCAAGGGCA
<i>Leptin</i>	Forward	ACCACCATTGTCACCAGGATCAA
<i>Leptin</i>	Reverse	ACCCTCTGCTTGGCGGATA
<i>PPARγ2</i>	Forward	AGTGTGAATTACAGCAAATCTCTGTTTT
<i>PPARγ2</i>	Reverse	GCACCATGCTCTGGGTCAA

Table S1: Primers for qPCR. Related to STAR Methods.